Supplementary Materials for

The principles of cascading power limits in small, fast biological and engineered systems

Mark Ilton, M. Saad Bhamla,* Xiaotian Ma,* Suzanne M. Cox,* Leah L. Fitchett, Yongjin Kim, Je-sung Koh, Deepak Krishnamurthy, Chi-Yun Kuo, Fatma Zeynep Temel, Alfred J. Crosby, Manu Prakash, Gregory P. Sutton, Robert J. Wood, Emanuel Azizi,† Sarah Bergbreiter,† S. N. Patek†‡

*These authors contributed equally to this work.
†These authors contributed equally to this work.
‡Corresponding author. Email: snp2@duke.edu

Published 27 April 2018, *Science* **360**, eaao1082 (2018)
DOI: 10.1126/aao1082

This PDF file includes:

Supplementary Text

We examine the kinematic performance of systems using simplified motor, spring, and latch models. The model components allow us to solve the dynamic equations of motion analytically, and in terms of non-dimensional variables set by the motor characteristics. Using this framework, the force output of the system is defined as a function of displacement and velocity and provides a system-level view of the dynamics. We compare systems driven by the same motor (a linear F-v trade-off motor), but with different combinations of springs and latches. In the main text of the paper, a motor-driven system with a linear force-velocity trade-off is compared to a spring-driven system involving the same motor but with a spring with non-zero mass ("heavy spring" here in the notation of the supplementary information) and a latch which has a rounded edge ("rounded latch" here).

The supplementary information is broken down into sections in which additional layers of complexity are added on piecewise to more fully explain the underlying modeling. In Section S1, we consider the system in which the motor directly drives a load mass projectile (shown schematically in Fig. 1B). Sections S2-S6 incorporate a spring (an ideal or heavy spring) and a latch (an ideal, rounded, or parabolic latch), which use the motor to pre-load energy into the spring; the load mass is then driven by the spring after unlatching occurs (the process is depicted schematically in Fig. 1C). The combinations of motor, spring, and latch are summarized in Table S1, listed along with their corresponding section number.

Section #	Motor	Spring	Latch
S1	linear F-v motor	-	-
S2	linear F-v motor	ideal spring	ideal latch
S3	linear F-v motor	heavy spring	ideal latch
S4	linear F-v motor	ideal spring	rounded latch
S5	linear F-v motor	ideal spring	parabolic latch
S6	linear F-v motor	heavy spring	parabolic latch

Table S1: Summary of the motor, spring, and latch combinations used in Sections S1-S6 of this document.

In Section S7, we demonstrate that for an ideal spring, there is a potential benefit for spring-driven motion if and only if the motor has a sufficient F-v trade-off. We define a "sufficient" F-v trade-off as one in which the force decreases as a function of velocity, and for which there exists a maximum velocity, such that force goes to zero above that velocity. Finally, in Section S8, we show that altering the load geometry has a similar effect to changing the latch geometry.

For mathematical simplicity and to demonstrate the generality of dynamics, we work in non-dimensional variables summarized in Table S2. Since we are comparing different configurations while holding the motor constant, we have chosen to non-dimensionalize in terms of the motor parameters: the maximum force of the motor ($F_{\max}$), the range-of-motion of the motor (d), and the maximum velocity of the motor ($v_{\max}$). We use the convention that non-dimensional variables are capped by the tilde accent symbol ($\tilde{\cdot}$). For example, the displacement, x, which has units of length, has a corresponding non-dimensional equivalent $\tilde{x}$.

Variable	Dimensionless variable
Force, F	$\tilde{f} = \frac{F}{F_{\max}}$
Velocity, v	$\tilde{v} = \frac{v}{v_{\max}}$
Displacement, x	$\tilde{x} = \frac{x}{d}$
Time, t	$\tilde{t} = t\frac{v_{\max}}{d}$
Mass, m	$\tilde{m} = m\frac{v_{\max}^2}{F_{\max}d}$

Table S2: Summary of non-dimensional variables used in this document.

Although the details of the models and the analytical equations of motion are detailed in Sections S1-S6, here we present a summary of the comparison between the different systems. To compare the six systems, there are several different output metrics that can be used. Three of these are shown in Fig. S1, the take-off velocity, the take-off duration, and the maximum power. The goal of a system might be to minimize take-off duration, maximize take-off velocity, and maximize take-off power (or some combination of these or other variables). These output variables depend on the load mass of the projectile, with heavier projectiles generally having a longer take-off duration with a smaller take-off velocity and smaller maximum power.

There are two important points demonstrated by the output from these models. First, the motor directly driving the load mass (Section S1) has a better performance for heavy masses, while the systems with a latch and spring (Sections S2-S6) outperform the motor for light loads. Intuitively, because light masses can be more easily be accelerated to high velocity, they push the velocity limits of the motor, which means a spring-driven system can be beneficial when driving light mass. There is a critical mass which lies at the cross-over in performance between the directly driven system and the spring-driven system. This critical mass depends on which spring and latch model are used, and it also depends on the output variable. For example, there is a cross-over in the take-off velocity of the motor + ideal spring + ideal latch (red dashed line in Fig. S1A) and the motor only (blue solid in in Fig. S1A) at $\tilde{m} \approx 2$, whereas the cross-over of the maximum power in Fig. S1C for these two systems occurs at $\tilde{m} \approx 4$. This dependence of the cross-over on the output variable relates to the second important point demonstrated by the models: for a given mass, choosing the system which optimizes one output variable does not necessarily optimize others. This is demonstrated by looking at the motor + heavy spring + ideal latch model (green dash-dotted line in Fig. S1), and observing that, at low mass, the take-off velocity and maximum power are inversely related.

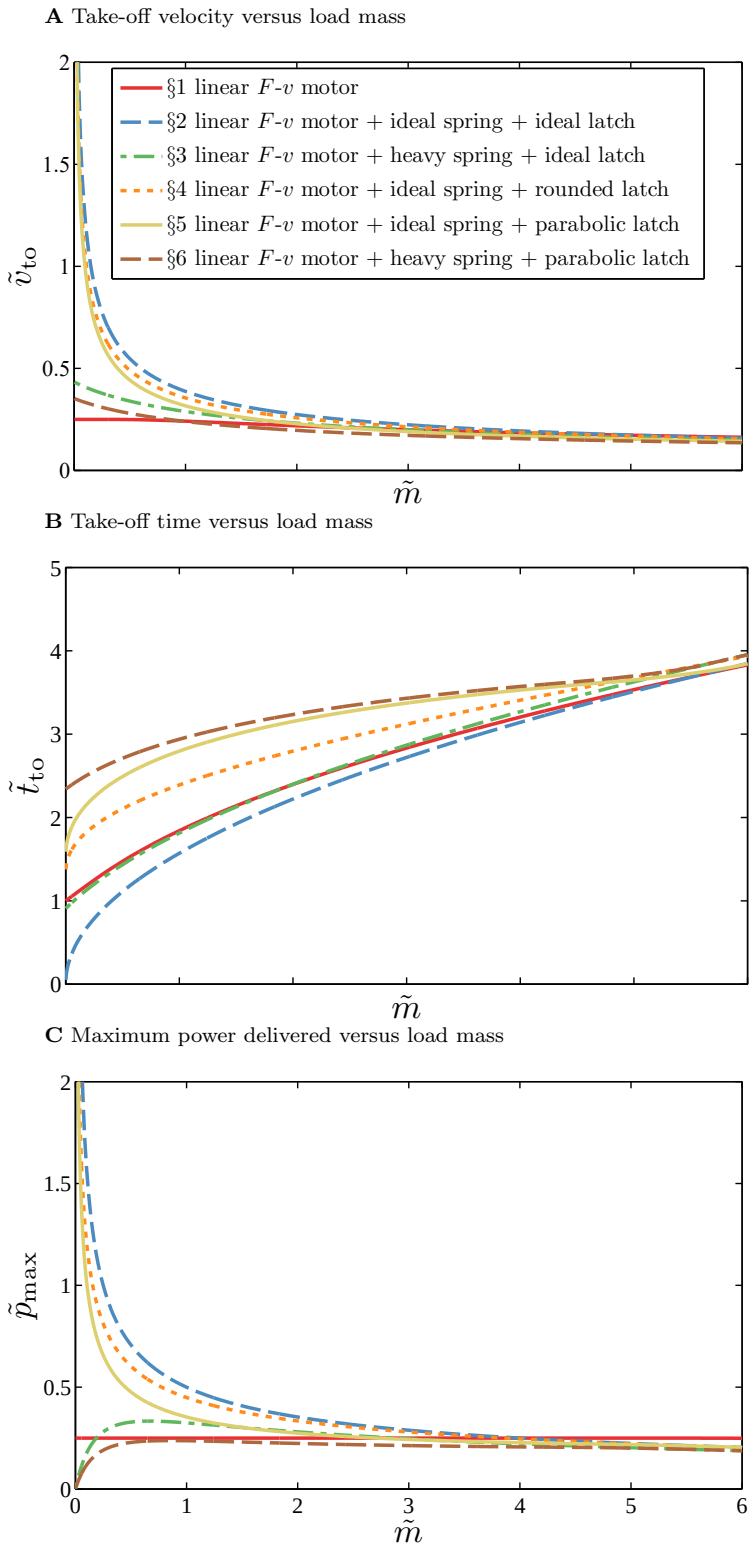

Figure S1: Summary of the results presented in Sections S1-S6. **A** The take-off velocity $\tilde{v}_{\mathrm{to}}$ of the load decreases as a function of its mass $\tilde{m}$. **B** the take-off time $\tilde{t}_{\mathrm{to}}$ increases with load mass. **C** The maximum power $\tilde{p}_{\mathrm{max}}$ delivered to the load mass diverges as $\tilde{m} \to 0$ for the three models with an ideal spring (Sections S2, S4-S5), remains constant when the motor directly drives the load mass (Section S1), and decreases at small loads when being driven by a heavy spring (Section S3, S6).

One way to visualize the system-level performance is by writing the output force of the system on the projectile as a function of displacement and velocity. Figure S2 shows the force-displacement-velocity $\tilde{f}(\tilde{x}, \tilde{v})$ characteristics of the models presented in Sections S1-S6. The magnitude of the force is plotted as a color gradient, along with the force contour lines shown in light gray. The phase-space trajectory $\tilde{v}(\tilde{x})$ of projectiles of different mass are shown as the thick black lines. The shape of the force-displacement-velocity relationship defines a field in which the different mass projectiles respond, giving rise to their trajectories. These trajectories define the characteristic output variables previously discussed in Fig. S1.

The effect of the latch on system-level performance is compared in Fig. S2(B,D,E). The latch geometry defines a region in the upper-left quadrant of phase space where the force abruptly falls to zero due to the geometric constraint of the latch. A more direct comparison is shown in Fig. S3. The different latches shape the energy release from the spring, and determine how much energy is transferred into the kinetic energy of the load mass. In the case of smooth, rigid surfaces between the latch and projectile, this release is determined solely by the geometry and speed of latch release, and not by the coefficient of friction between the surfaces.

A §S1 linear F-v motor

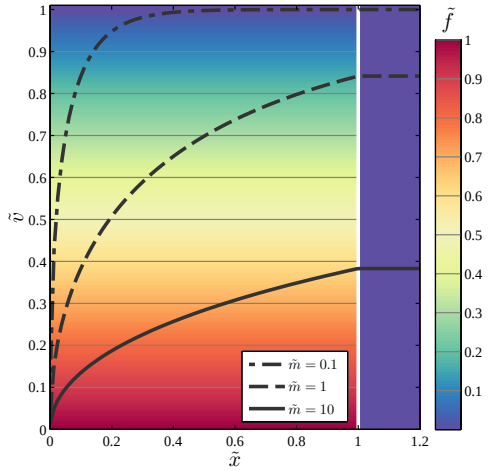

B §S2 linear F-v motor + ideal spring + ideal latch

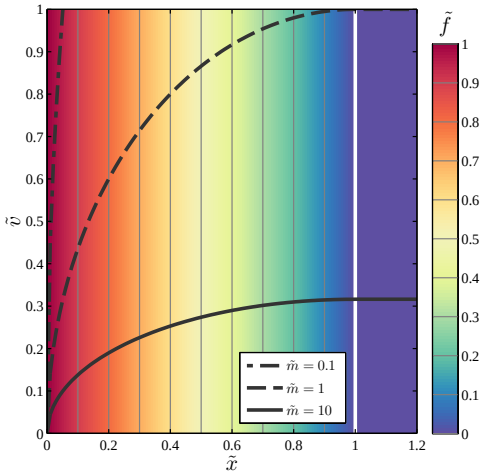

C §S3 linear F-v motor + heavy spring + ideal latch

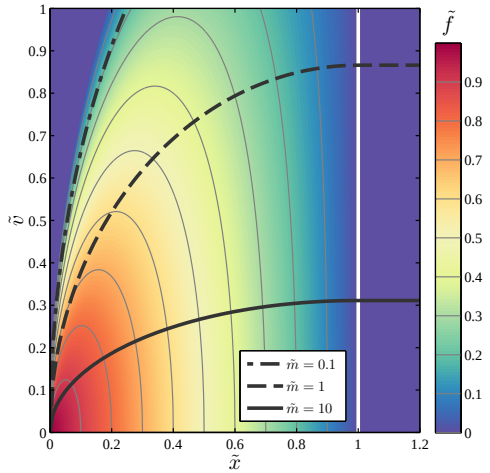

D §S4 linear F-v motor + ideal spring + rounded latch

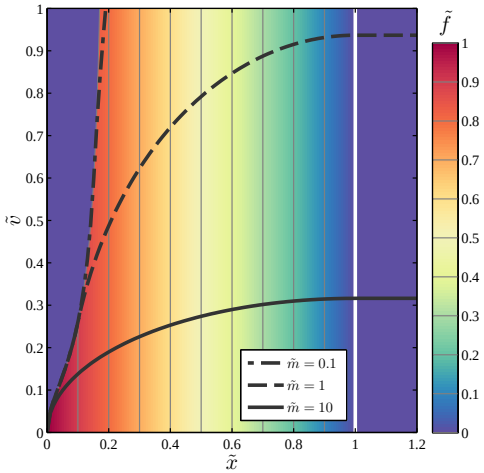

E §S5 linear F-v motor + ideal spring + parabolic latch

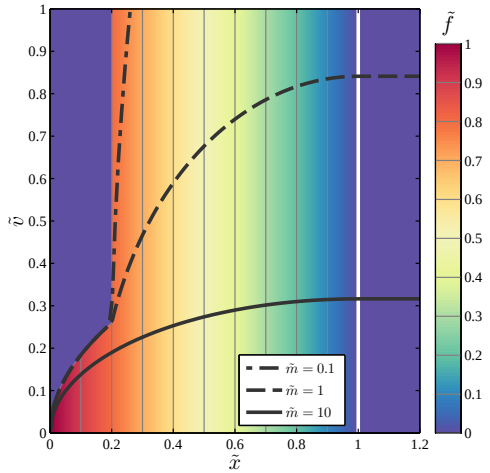

F §S6 linear F-v motor + heavy spring + parabolic latch

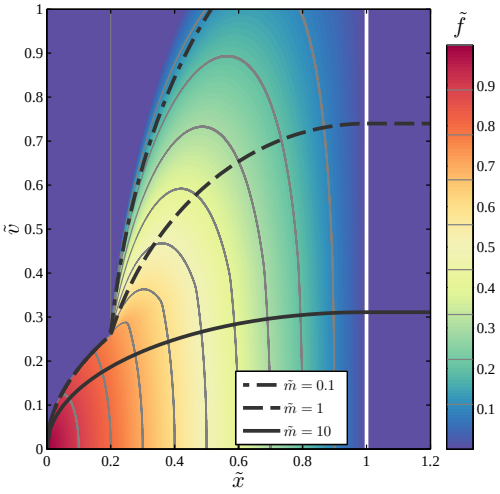

Figure S2: **A-F** Comparison of $\tilde{f}(\tilde{x}, \tilde{v})$ output for the models presented in Sections S1-S6.

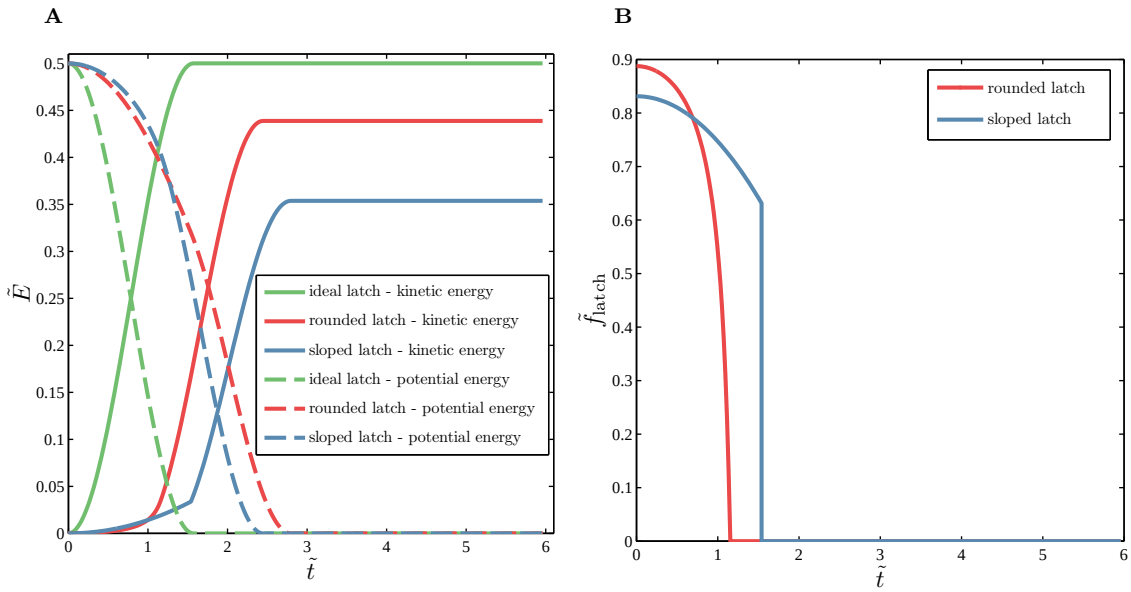

Figure S3: Energy release and latching force from the three different latches used with an ideal spring discussed in Sections S2, S4, and S5. **A** The energy stored in the spring (potential energy) and released (kinetic energy) as a function of time. **B** The shape of the latch determines the rate of energy release, and the latching force profile. For the ideal latch, the latching force falls to zero immediately at $\tilde{t} = 0$, while the rounded and parabolic latch have a finite unlatching time.

Section S1 - Linear F-v motor

In the first system, we considered a linear F-v motor directly driving a load mass, m, as in Fig. 2a of the main text, Newton's second law gives

$$F(v) = F_{\max}\left(1 - \frac{v}{v_{\max}}\right) = m\frac{dv}{dt}, \tag{1}$$

subject to the initial condition $x(t = 0) = v(t = 0) = 0$. Eq.(1) is valid for the range of motion of the motor, namely, when $0 \leq x \leq d$. For $x > d$, $F = 0$, and the velocity of the load mass is constant and equal to its take-off velocity $v(t > t_{\text{to}}) = v_{\text{to}}$. Here t_{to} is defined as the time to release, with $x(t_{\text{to}}) = d$. If we non-dimensionalize Eq.(1) by defining

$$\tilde{f} = \frac{F}{F_{\max}}$$
$$\tilde{v} = \frac{v}{v_{\max}}$$
$$\tilde{x} = \frac{x}{d}$$
$$\tilde{t} = t\frac{v_{\max}}{d},$$
$$\tilde{m} = m\frac{v_{\max}^2}{F_{\max}d}$$

then the differential equation describing the motion of the load mass can be written as

$$\tilde{f}(\tilde{v}) = 1 - \tilde{v} = \tilde{m}\frac{d\tilde{v}}{d\tilde{t}}. \tag{2}$$

The solution to Eq. (2) is

$$\tilde{v} = 1 - e^{-\tilde{t}/\tilde{m}}, \tag{3}$$

which gives the displacement before take-off as

$$\tilde{x} = \tilde{t} + \tilde{m}\left(e^{-\tilde{t}/\tilde{m}} - 1\right). \tag{4}$$

The condition for take-off requires $\tilde{x}(\tilde{t} = \tilde{t}_{\text{to}}) = 1$, which means that t_{to} can be solved as a function $\tilde{m}$ as

$$1 = \tilde{t}_{\text{to}} + \tilde{m}\left(e^{-\tilde{t}_{\text{to}}/\tilde{m}} - 1\right), \tag{5}$$

the numerical solution to which is shown as the solid blue line in the middle panel of Fig. S1. This sets the take-off velocity as $\tilde{v}_{\text{to}} = \tilde{v}(\tilde{t}_{\text{to}})$, which can be written in terms of $\tilde{t}_{\text{to}}$

$$\tilde{v}_{\text{to}} = \frac{\tilde{t}_{\text{to}} - 1}{\tilde{m}},$$

and defines two regimes for the kinematics (before and after take-off) as

$$\tilde{x}(\tilde{t}) = \begin{cases} \tilde{t} + \tilde{m}\left(e^{-\tilde{t}/\tilde{m}} - 1\right) & \text{if } \tilde{t} \leq \tilde{t}_{\text{to}} \\ \tilde{t}_{\text{to}} + e^{-\tilde{t}_{\text{to}}} - 1 + \tilde{v}_{\text{to}}(\tilde{t} - \tilde{t}_{\text{to}}) & \text{if } \tilde{t} > \tilde{t}_{\text{to}} \end{cases} \tag{6}$$

$$\tilde{v}(\tilde{t}) = \begin{cases} 1 - e^{-\tilde{t}/\tilde{m}}, & \text{if } \tilde{t} \leq \tilde{t}_{\text{to}} \\ \tilde{v}_{\text{to}} & \text{if } \tilde{t} > \tilde{t}_{\text{to}} \end{cases} \tag{7}$$

$$\tilde{f}(\tilde{t}) = \begin{cases} e^{-\tilde{t}/\tilde{m}}, & \text{if } \tilde{t} \leq \tilde{t}_{\text{to}} \\ 0 & \text{if } \tilde{t} > \tilde{t}_{\text{to}} \end{cases} \tag{8}$$

The non-dimensional power output $\tilde{p} = \tilde{f} \cdot \tilde{v}$, is

$$\tilde{p}(\tilde{t}) = \begin{cases} e^{-\tilde{t}/\tilde{m}} - e^{-2\tilde{t}/\tilde{m}}, & \text{if } \tilde{t} \leq \tilde{t}_{\text{to}} \\ 0 & \text{if } \tilde{t} > \tilde{t}_{\text{to}}. \end{cases} \tag{9}$$

The maximum power, $\max(\tilde{p}(\tilde{t}))$ is constant for small load masses (the peak of the $\tilde{p}(\tilde{t})$ plot in Fig. S4), with $\tilde{p}_{\max} = 0.25$ for $\tilde{m} < \frac{1}{\ln(2)-1/2} \approx 5.18$. Otherwise $\tilde{p}_{\max} = \tilde{p}(\tilde{t}_{\text{to}})$.

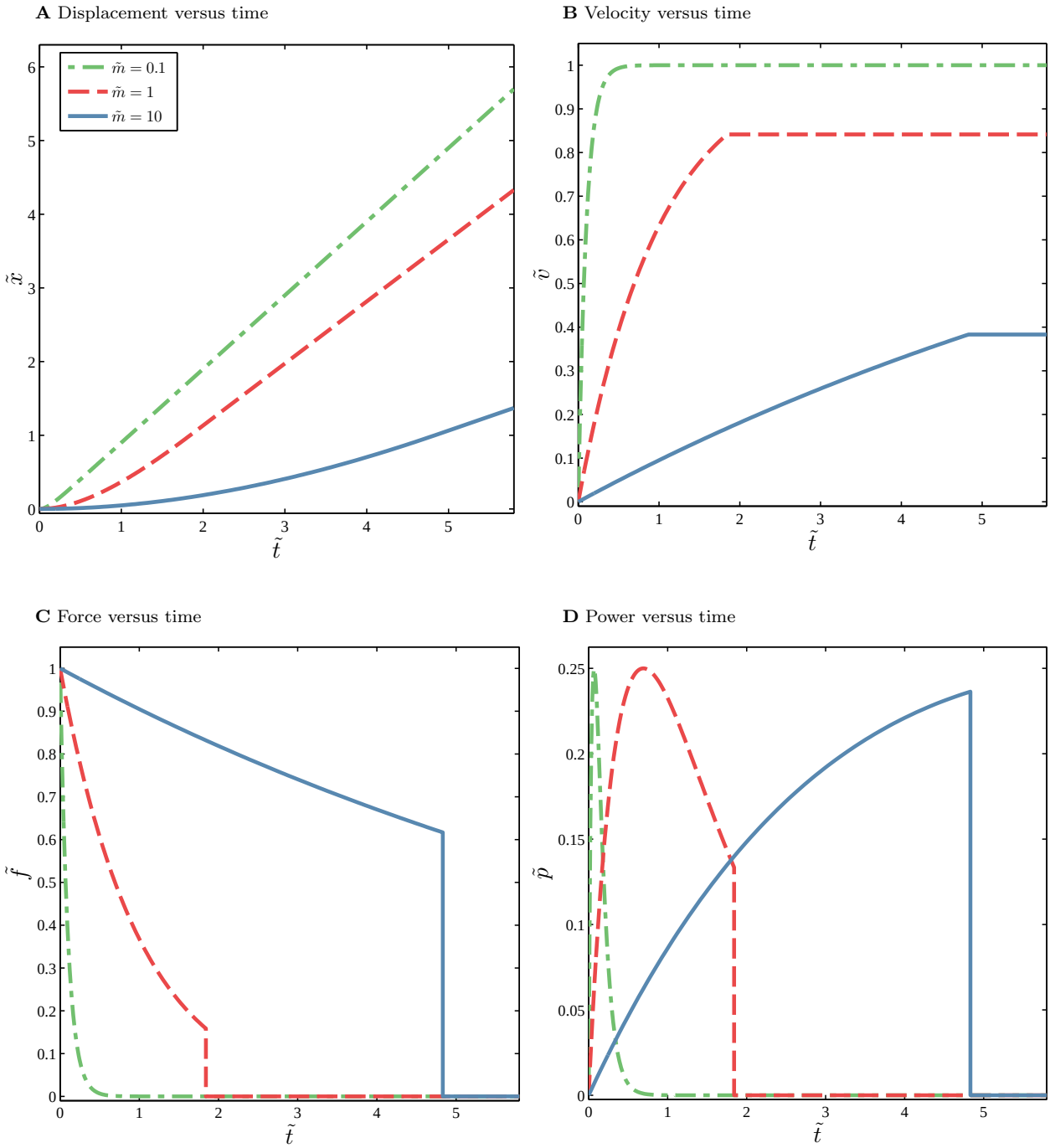

Figure S4: Dynamics of a system with a linear motor used to directly drive the load mass shown for **A** displacement, **B** velocity, **C** force, and **D** power. The dynamics are given by Eqs. (6-9).

The take-off velocity is a function of mass through its dependence on $\tilde{t}_{\mathrm{to}}$; $\tilde{v}_{\mathrm{to}}(\tilde{m})$ is shown in Fig. S1.

Section S2 - Linear F-v motor + ideal spring + ideal latch

For an ideal spring slowly loaded to a maximum force $F_{\max} = kd$, and then released with load mass m, the equations of motion of the load mass before take-off are

$$x(t) = d\left(1 - \cos\left(\sqrt{\frac{k}{m}}\, t\right)\right)$$

$$v(t) = d\sqrt{\frac{k}{m}} \sin\left(\sqrt{\frac{k}{m}}\, t\right)$$

$$F(t) = kd\cos\left(\sqrt{\frac{k}{m}}\, t\right) = k(d - x),$$

where the spring is assumed to be Hookean, has no force-velocity trade-off, is massless, and does not lose any energy to the latch. These equations of motion are valid during the launch of the projectile, namely for $t < t_{\text{to}}$.

The non-dimensional form of these equations of motion of the load mass before take-off (using the same non-dimensionalization as in Section S1) are

$$\tilde{x}(\tilde{t}) = \left(1 - \cos\left(\tilde{v}_{\text{to}}\tilde{t}\right)\right) \tag{10}$$

$$\tilde{v}(\tilde{t}) = \tilde{v}_{\text{to}} \sin\left(\tilde{v}_{\text{to}}\tilde{t}\right) \tag{11}$$

$$\tilde{f}(\tilde{t}) = \tilde{m}\tilde{v}_{\text{to}}^2 \cos\left(\tilde{v}_{\text{to}}\tilde{t}\right) \tag{12}$$

$$\tilde{p}(\tilde{t}) = \tilde{f} \cdot \tilde{v} = \frac{\tilde{m}\tilde{v}_{\text{to}}^3}{2} \sin\left(2\tilde{v}_{\text{to}}\tilde{t}\right), \tag{13}$$

where

$$\tilde{v}_{\text{to}} = \frac{1}{\sqrt{\tilde{m}}}. \tag{14}$$

Setting $\tilde{v}_{\text{to}}\tilde{t}_{\text{to}} = \pi/2$ to maximize $\tilde{v}$ gives the take-off time

$$\tilde{t}_{\text{to}} = \frac{\pi\sqrt{\tilde{m}}}{2}.$$

The maximum power occurs when $\tilde{t} = \tilde{t}_{\text{to}}/2$, with

$$\tilde{p}_{\max} = \frac{1}{2\sqrt{\tilde{m}}}.$$

The force can be written in terms of x as

$$\tilde{f} = 1 - \tilde{x} \tag{15}$$

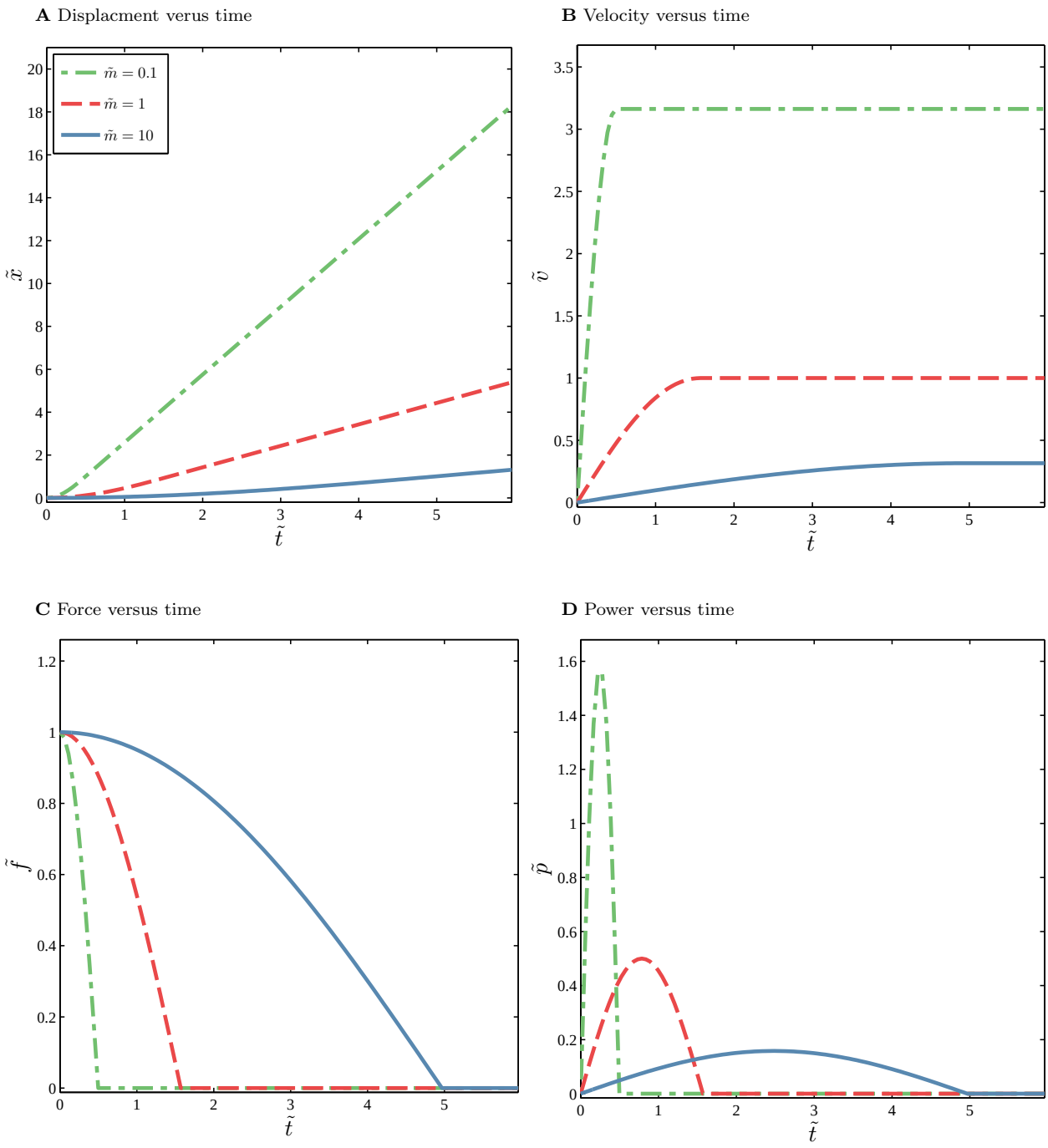

Figure S5: Dynamics of a system with a linear motor, ideal spring and ideal latch shown for **A** displacement, **B** velocity, **C** force, and **D** power. The dynamics are given by Eqs. (10-13).

Section S3 - Linear F-v motor + heavy spring + ideal latch

In this section we make a minor modification to the previous section: the Hookean spring is considered to have a non-zero mass. By considering a heavy spring, complicated effects such as the spatially non-uniform release of strain energy due to elastic wave propagation and inhomogeneity in the spring mass distribution can arise. Here a simplified approach is used where both the mass distribution in the spring and strain energy release are assumed to be spatially uniform.

With these assumptions, the dynamics of the heavy spring can be derived by considering an energy balance: setting the work done by the spring equal to the total change in kinetic energy. The total kinetic energy of the system depends on the position of the load mass, $K_{\text{tot}} = K_{\text{tot}}(x)$. There is a contribution to K_{tot} from the load mass ($\frac{1}{2}mv^2$), and the kinetic energy of the spring given by

$$K_s(x) = \int_{-(L_0-d)}^{x} \frac{1}{2}\lambda(x) v_s(x';x)^2 \, dx', \tag{16}$$

where $v_s(x';x)$ is the velocity of the spring at point x' given that the load mass is at point x, and L_0 is the equilibrium length of the spring ($L_0 = L(x = d)$). The linear mass density of the spring, $\lambda(x)$, is related to the total mass of the spring, m_s, and length of spring $L(x)$ by

$$\lambda(x) = \frac{m_s}{L(x)} = \frac{m_s}{x + L_0 - d}. \tag{17}$$

The expression in Eq.(16) can be evaluated using the assumption of a spatially uniform release of strain energy, which implies that there is a linear velocity distribution in the spring. The velocity goes to zero for the end of the spring connected to the ground,

$$v_s(-(L_0 - d); x) = 0,$$

and the velocity of the end of the spring connected to the load mass is equal to the velocity of the load mass $v(x)$, with

$$v_s(x; x) = v(x).$$

Using these two boundary conditions and the assumption of a linear velocity distribution in the spring, gives the spring velocity at point x' given the projectile is at point x as

$$v_s(x';x) = \frac{x' + L_0 - d}{x + L_0 - d}. \tag{18}$$

Substituting Eq.(18) into Eq.(16) and using Eq.(17), gives the kinetic energy of the spring

$$K_s(x) = \frac{m_s v(x)^2}{2(x + L_0 - d)^3} \int_{-(L_0-d)}^{x} (x' + L_0 - d)^2 \, dx' = \frac{m_s v(x)^2}{6},$$

which simplifies to

$$K_s(x) = \frac{m_s v(x)^2}{6}. \tag{19}$$

This gives the total kinetic energy as

$$K_{\text{tot}}(x) = \frac{1}{2}(m + \frac{m_s}{3})v(x)^2. \tag{20}$$

Assuming a conservation of energy, at take-off the total kinetic energy $K_{\text{tot}}(x = d)$ is equal to the potential energy stored in the spring by the motor $F_{\max}d/2$. This gives the take-off velocity $v_{\text{to}} = v(x = d)$ in terms of the properties of the system as

$$v_{\text{to}} = \sqrt{\frac{F_{\max} d}{m + m_s/3}}.$$

Dividing both sides by $v_{\max}$ non-dimensionalizes the take-off velocity

$$\tilde{v}_{\text{to}} = \sqrt{\frac{1}{\tilde{m} + \frac{\tilde{m}_s}{3}}}, \tag{21}$$

where we have introduced the non-dimensional spring mass $\tilde{m}_s = \frac{m_s v_{\max}^2}{F_{\max} d}$. The non-dimensional equations of motion until take-off are the same as the ideal spring case [Eq.(10-13)] but with $\tilde{v}_{\text{to}}$ defined by Eq.(21):

$$\tilde{x}(\tilde{t}) = \left(1 - \cos\left(\tilde{v}_{\text{to}}\tilde{t}\right)\right) \tag{22}$$

$$\tilde{v}(\tilde{t}) = \tilde{v}_{\text{to}} \sin\left(\tilde{v}_{\text{to}}\tilde{t}\right) \tag{23}$$

$$\tilde{f}(\tilde{t}) = \tilde{m}\tilde{v}_{\text{to}}^2 \cos\left(\tilde{v}_{\text{to}}\tilde{t}\right) \tag{24}$$

$$\tilde{p}(\tilde{t}) = \tilde{f} \cdot \tilde{v} = \frac{\tilde{m}\tilde{v}_{\text{to}}^3}{2} \sin\left(2\tilde{v}_{\text{to}}\tilde{t}\right), \tag{25}$$

The take-off time can be solved for by setting $\tilde{v}_{\text{to}}\tilde{t}_{to} = \pi/2$ which yields

$$\tilde{t}_{\text{to}} = \frac{\pi\sqrt{\tilde{m} + \frac{\tilde{m}_s}{3}}}{2},$$

and the maximum power occurs when $\tilde{v}_{\text{to}}\tilde{t} = \pi/4$ and equals

$$\tilde{p}_{\max} = \frac{\tilde{m}}{2(\tilde{m} + \frac{\tilde{m}_s}{3})^{3/2}}.$$

To rewrite $\tilde{f}(\tilde{t}; \tilde{m})$ in terms of normalized displacement and velocity $\tilde{f}(\tilde{x}, \tilde{v})$, we can rearrange Eq.(21) to substitute in for $\tilde{m}$ in terms of $\tilde{v}_{\text{to}}$ and $\tilde{m}_s$. We also use the expression for $\tilde{x}(t)$ to replace the cosine term, giving,

$$\tilde{f}(\tilde{t}) = \left(1 - \frac{\tilde{m}_s\tilde{v}_{\text{to}}^2}{3}\right)(1 - \tilde{x}).$$

Finally, by using $\sin^2 + \cos^2 = 1$ with $\tilde{x}(\tilde{t})^2 + \tilde{v}(\tilde{t})^2$, we can eliminate $\tilde{v}_{\text{to}}^2 = \frac{\tilde{v}^2}{1-(1-\tilde{x}^2)}$, which results in the final expression for $\tilde{f}(\tilde{x}, \tilde{v})$

$$\tilde{f}(\tilde{x}, \tilde{v}) = \left(1 - \frac{\tilde{m}_s\tilde{v}^2}{3\left(1 - (1 - \tilde{x})^2\right)}\right)(1 - \tilde{x}) \tag{26}$$

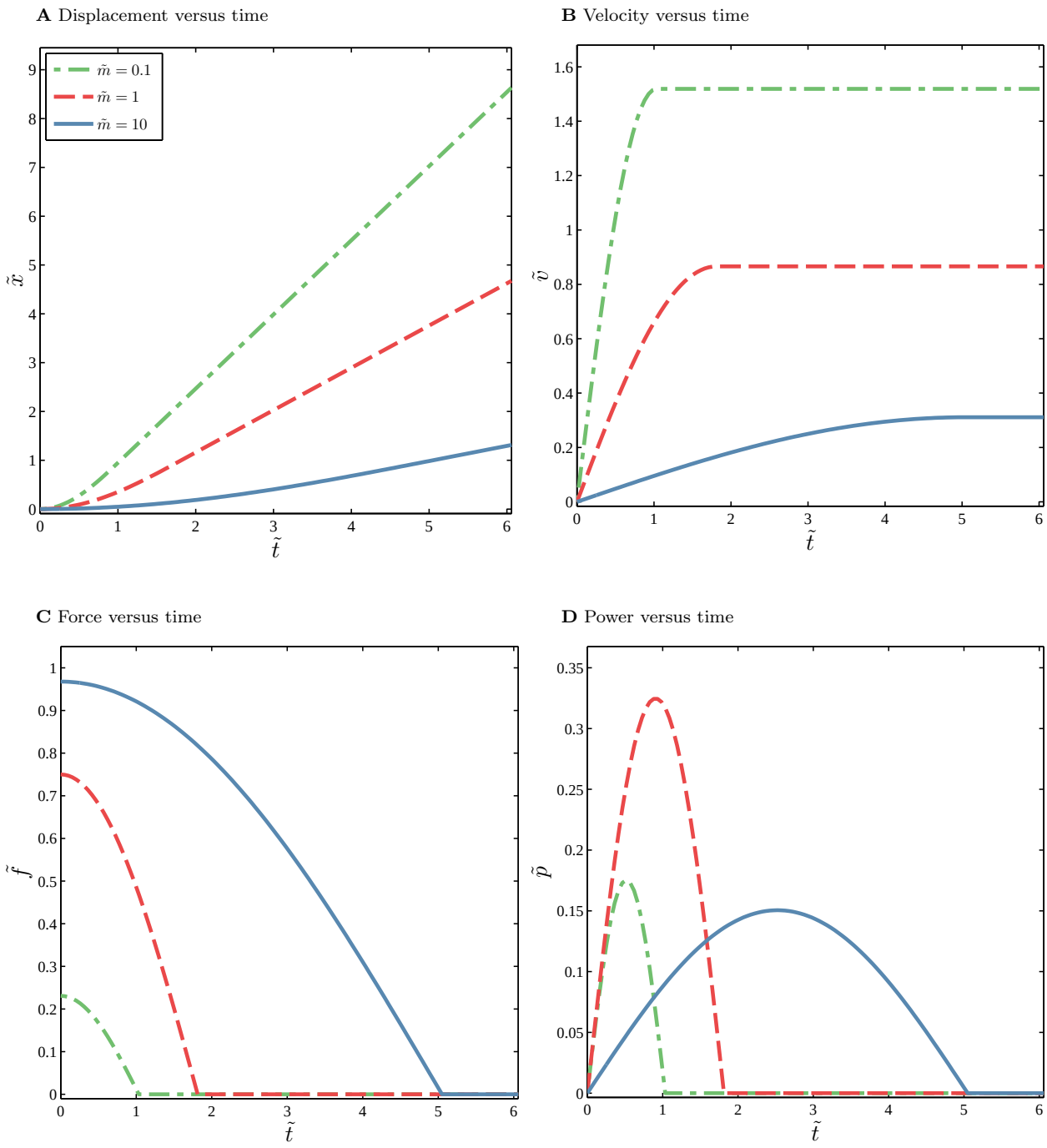

Figure S6: Dynamics of a system with a linear motor, heavy spring and ideal latch shown for **A** displacement, **B** velocity, **C** force, and **D** power. The mass of the spring is set to $\tilde{m}_s = 1$. The dynamics are given by Eqs. (22-25).

Section S4 - Linear F-v motor + ideal spring + rounded latch

In previous sections, we considered the latch to be ideal: an obstruction with frictionless surfaces and perfectly sharp edges is removed instantaneously at $t = 0$. In the next two sections, we consider the effect of the latch by altering the latch geometry (Fig. S7) and removing the latch with a finite constant velocity v_L. In this analysis, the latches are still considered to be frictionless, and the effect of geometric constraint on the kinematics of release will be examined.

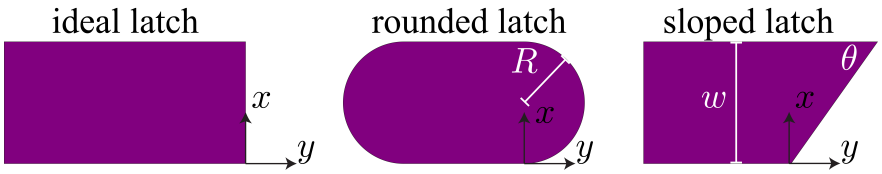

Figure S7: Examples of different latch geometries.

In the unlatching of the rounded latch shown in Fig. S8, the latch force F_{latch} from each of the two sides of the latch initially balances the spring force F_{spring}. When unlatching begins, there exists a force normal to the latch surface at the point of contact between the mass and the latch. The force is purely normal to the surface due to the frictionless contact. At some point in time $t = t_\ell$, the normal force exerted by the latch onto the mass falls to zero, and the mass is released from the latch at position $x = x_\ell$ with a velocity $v = v_\ell$. In this section, we will develop equations describing the motion of the mass before latch release ($t < t_\ell$) and after latch release ($t > t_\ell$).

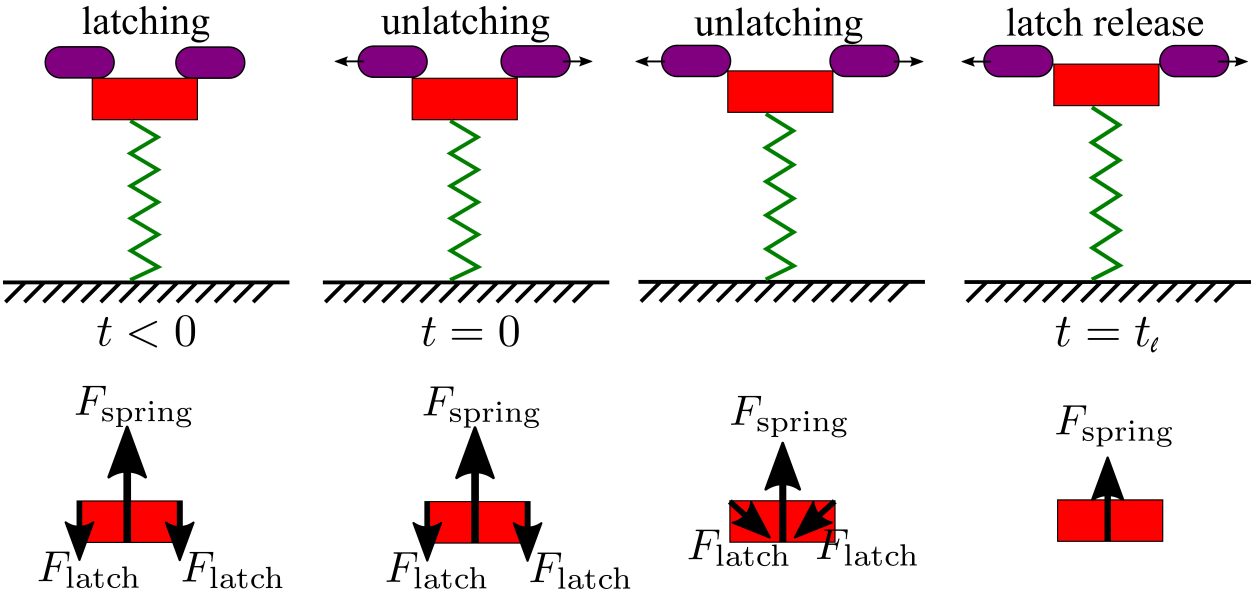

Figure S8: Schematic depiction of the unlatching process, and the balance of the latching force (F_{latch}) being counteracted by the spring force (F_{spring}).

Before latch release ($t < t_\ell$)

For the mass in contact with the rounded latch, the motion could be analyzed using the equations of motion in a polar coordinate system. Here we take a more general approach which will allow the analysis of more complicated latch geometries which don't have a constant radius of curvature.

To be consistent with previous sections, we choose a co-ordinate system for the latch geometry where x is the vertical direction and y is the horizontal direction in Fig. S8. By symmetry we consider here only one side of the latch, taking $x = 0$ to be initial position of the top surface of the mass, and $y = 0$ to be the point

at which the latch begins to curve, such that the surface of the latch is described by the function

$$x = R\left(1 - \sqrt{1 - \left(\frac{y}{R}\right)^2}\right).$$

Assuming the latch is pulled away with a constant velocity v_L, the position of the mass when in contact with the latch is given by setting $y = v_L t$

$$x(t) = R\left(1 - \sqrt{1 - \left(\frac{v_L t}{R}\right)^2}\right). \tag{27}$$

Taking the derivative of Eq. (27) with respect to time yields the velocity of the mass when in contact with the latch

$$v(t) = v_L \frac{\left(\frac{v_L t}{R}\right)}{\sqrt{1 - \left(\frac{v_L t}{R}\right)^2}}. \tag{28}$$

By taking $F_{\text{net}} = m\frac{dv}{dt}$, the net force acting on the mass by the spring and latch is

$$F(t) = m\frac{\left(\frac{v_L^2}{R}\right)}{\left(1 - \left(\frac{v_L t}{R}\right)^2\right)^{3/2}}. \tag{29}$$

Equations (27-29) are valid for when the mass is in contact with the latch, namely $t < t_\ell$. To determine when these equations are valid we need to solve for when the latching force goes to zero, and $F_{\text{net}} = F_{\text{spring}}$. Using Eq.(29) and $F_{\text{spring}} = F_{\max}\left(1 - \frac{x(t)}{d}\right)$ gives an expression which can be solved numerically for $t_\ell(F_{\max}, m, R, d, v_L)$

$$F_{\max}\left(1 - \frac{R}{d}\left(1 - \sqrt{1 - \left(\frac{v_L t_\ell}{R}\right)^2}\right)\right) = m\frac{\left(\frac{v_L^2}{R}\right)}{\left(1 - \left(\frac{v_L t_\ell}{R}\right)^2\right)^{3/2}} \tag{30}$$

To put these equations in non-dimensional form we let $\tilde{R} = R/d$, $\tilde{v}_\ell = v_L/v_{\max}$, and $\tilde{t}_\ell = t_\ell \frac{v_{\max}}{d}$. This gives $\tilde{t}_\ell(\tilde{m}, \tilde{R}, \tilde{v}_\ell)$ implicitly as

$$\left(1 - \left(\frac{\tilde{v}_\ell \tilde{t}_\ell}{\tilde{R}}\right)^2\right)^{3/2}\left(1 - \tilde{R}\left(1 - \sqrt{1 - \left(\frac{\tilde{v}_\ell \tilde{t}_\ell}{\tilde{R}}\right)^2}\right)\right) = \frac{\tilde{m}\tilde{v}_\ell^2}{\tilde{R}}.$$

The kinematic equations of motion for $\tilde{t} < \tilde{t}_\ell$ are

$$\tilde{x}(\tilde{t}) = \tilde{R}\left(1 - \sqrt{1 - \left(\frac{\tilde{v}_\ell \tilde{t}}{\tilde{R}}\right)^2}\right), \tag{31}$$

$$\tilde{v}(\tilde{t}) = \tilde{v}_\ell \frac{\left(\frac{\tilde{v}_\ell \tilde{t}}{\tilde{R}}\right)}{\sqrt{1 - \left(\frac{\tilde{v}_\ell \tilde{t}}{\tilde{R}}\right)^2}}. \tag{32}$$

$$\tilde{f}(\tilde{t}) = \frac{\left(\frac{\tilde{m}\tilde{v}_\ell^2}{\tilde{R}}\right)}{\left(1 - \left(\frac{\tilde{v}_\ell \tilde{t}}{\tilde{R}}\right)^2\right)^{3/2}}. \tag{33}$$

$$\tilde{p}(\tilde{t}) = \frac{\left(\frac{\tilde{m}\tilde{v}_\ell^3}{\tilde{R}}\right)\left(\frac{\tilde{v}_\ell \tilde{t}}{\tilde{R}}\right)}{\left(1 - \left(\frac{\tilde{v}_\ell \tilde{t}}{\tilde{R}}\right)^2\right)^2}. \tag{34}$$

For large masses, $\tilde{t}_\ell \to 0$, which occurs when the latching force goes to zero for $\tilde{t} = 0$. This happens for all $\tilde{m} > \tilde{m}_c$, where

$$\tilde{m}_c = \frac{\tilde{m}}{\tilde{f}(\tilde{t}=0)} = \frac{\tilde{R}}{\tilde{v}_\ell^2}$$

In other words, for $\tilde{m} > \tilde{R}/\tilde{v}_\ell^2$, the unlatching time goes to zero with $\tilde{t}_\ell = \tilde{x}_\ell = \tilde{v}_\ell = 0$, and the latch behaves as an ideal latch.

An alternate way to write the velocity $\tilde{v}$ is in terms of displacement

$$\tilde{v} = \tilde{v}_\ell \frac{\sqrt{1 - \left(1 - \frac{\tilde{x}}{\tilde{R}}\right)^2}}{1 - \frac{\tilde{x}}{\tilde{R}}}.$$

Notably, the kinematics of the mass during the unlatching phase are independent of its mass, and therefore the velocity-displacement trajectory is entirely determined by the geometry and speed of the latch release.

After latch release ($t > t_\ell$)

After the latch has released, the motion of the mass before take-off is the first quarter of a harmonic oscillation cycle determined by the initial conditions $\tilde{x}_\ell = \tilde{x}(\tilde{t}_\ell)$ and $\tilde{v}_\ell = \tilde{v}(\tilde{t}_\ell)$. The take-off velocity $\tilde{v}_{\text{to}}$ can be determined by requiring the conservation of energy

$$\frac{1}{2}\tilde{m}\tilde{v}_\ell^2 + \frac{1}{2}\left(1 - \tilde{x}_\ell\right)^2 = \frac{1}{2}\tilde{m}\tilde{v}_{\text{to}}^2.$$

The equations of motion for $\tilde{t} > \tilde{t}_\ell$ can be written in terms of $\tilde{v}_{\text{to}}$ as

$$\tilde{x}(\tilde{t}) = 1 - \sqrt{\tilde{m}}\tilde{v}_{\text{to}} \cos\left(\frac{\tilde{t}}{\sqrt{\tilde{m}}} + \tilde{\phi}\right) \tag{35}$$

$$\tilde{v}(\tilde{t}) = \tilde{v}_{\text{to}} \sin\left(\frac{\tilde{t}}{\sqrt{\tilde{m}}} + \tilde{\phi}\right) \tag{36}$$

$$\tilde{f}(\tilde{t}) = \sqrt{\tilde{m}}\tilde{v}_{\text{to}} \cos\left(\frac{\tilde{t}}{\sqrt{\tilde{m}}} + \tilde{\phi}\right) \tag{37}$$

$$\tilde{p}(\tilde{t}) = \frac{\sqrt{\tilde{m}}\tilde{v}_{\text{to}}^2}{2} \sin\left(2\left(\frac{\tilde{t}}{\sqrt{\tilde{m}}} + \tilde{\phi}\right)\right) \tag{38}$$

with the non-dimensional take-off velocity $\tilde{v}_{\text{to}}$ and phase $\tilde{\phi}$ given by the initial conditions $\tilde{x}_\ell$, $\tilde{v}_\ell$, $\tilde{t}_\ell$ as

$$\tilde{v}_{\text{to}} = \sqrt{\frac{\left(1 - \tilde{x}_\ell\right)^2}{\tilde{m}} + \tilde{v}_\ell^2} \tag{39}$$

$$\tilde{\phi} = \arctan\left(\frac{\sqrt{\tilde{m}}\tilde{v}_\ell}{1 - \tilde{x}_\ell}\right) - \frac{\tilde{t}_\ell}{\sqrt{\tilde{m}}} \tag{40}$$

The take-off time occurs at the maximum of $\tilde{v}(\tilde{t})$, when $\frac{\tilde{t}_{\text{to}}}{\sqrt{\tilde{m}}} + \tilde{\phi} = \frac{\pi}{2}$,

$$\tilde{t}_{\text{to}} = \frac{\pi\sqrt{\tilde{m}}}{2} - \sqrt{\tilde{m}} \arctan\left(\frac{\sqrt{\tilde{m}}\tilde{v}_\ell}{1 - \tilde{x}_\ell}\right) + \tilde{t}_\ell. \tag{41}$$

and the force after unlatching can be written solely in terms of $\tilde{x}$ as

$$\tilde{f} = 1 - \tilde{x}. \tag{42}$$

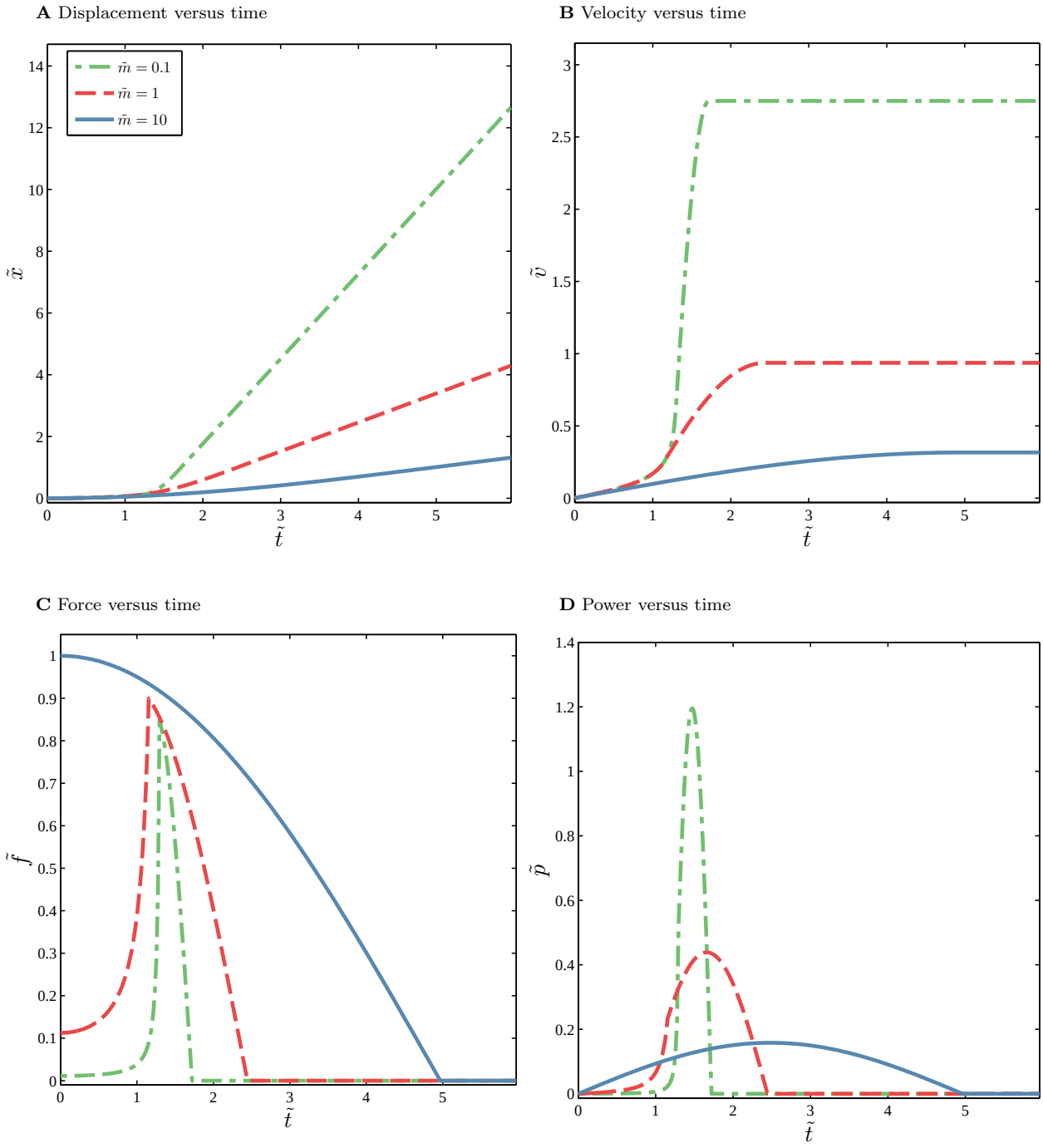

Figure S9: Dynamics of a system with a linear motor, ideal spring and rounded latch shown for **A** displacement, **B** velocity, **C** force, and **D** power. The normalized radius of curvature is set to $\tilde{R} = 0.2$ and the velocity of the latch $\tilde{v}_\ell = 0.15$. The curves are plotted from Eqs. (31-34) for $\tilde{t} < \tilde{t}_\ell$ and Eqs. (35-38) for $\tilde{t} > \tilde{t}_\ell$.

Section S5 - Linear F-v motor + ideal spring + parabolic latch

Similar to the previous section, here we consider altering the geometry of the latch by using an approximation to the sloped latch in Fig. S7. A parabolic-shaped latch will be used as an approximation to the sloped geometry due to the mathematical discontinuities induced by the sharp corner of the sloped latch, as described at the beginning of this section. The same general procedure from the previous section applies: determine the latch release time t_ℓ by solving for when the normal force of the latch goes to zero. This separates the dynamics into two stages, before and after latch release.

The geometry of a sloped latch can be simply described by

$$x = y \tan\theta,$$

for $x < w$. If the latch is pulled away with a constant velocity v_L, then

$$x(t) = \begin{cases} (v_L \tan\theta)\, t, & \text{if } t > 0 \\ 0 & \text{if } t < 0 \end{cases}$$

$$v(t) = \begin{cases} v_L \tan\theta, & \text{if } t > 0 \\ 0 & \text{if } t < 0 \end{cases}$$

$$F(t) = m v_L \tan\theta \delta(t),$$

where δ is the Dirac delta function. This functional form is problematic as the sharp corner of the latch at $(x = 0, y = 0)$ requires an infinite force for the mass to remain in contact with the latch. To avoid this, we introduce a rounded corner to the latch edge at $(x = 0, y = 0)$ by introducing a quadratic (parabolic) latch geometry which describes the latch geometry for $0 < x < w$ and $y > 0$

$$x = \frac{\tan^2\theta}{4w} y^2.$$

The prefactors are chosen such that the slope of the latch $\frac{dx}{dy}$ at $x = w$ is equal to $\tan\theta$. If this latch is pulled away with a constant velocity v_L at $t = 0$, then $y = v_L t$ and the position of the mass when in contact with the latch is (in non-dimensional units)

$$\tilde{x}(\tilde{t}) = \frac{\tilde{v}_\ell^2 \tan^2\theta}{4\tilde{w}} \tilde{t}^2, \tag{43}$$

where $\tilde{w} = w/d$ and $\tilde{v}_\ell = v_L/v_{\max}$. The other kinematic equations are

$$\tilde{v}(\tilde{t}) = \frac{\tilde{v}_\ell^2 \tan^2\theta}{2\tilde{w}} \tilde{t} \tag{44}$$

$$\tilde{f}(\tilde{t}) = \tilde{m} \frac{\tilde{v}_\ell^2 \tan^2\theta}{2\tilde{w}}. \tag{45}$$

$$\tilde{p}(\tilde{t}) = \tilde{m} \frac{\tilde{v}_\ell^4 \tan^4\theta}{4\tilde{w}^2} \tilde{t}. \tag{46}$$

The width of the latch w sets a maximum limit on the time it takes to unlatch $\tilde{t}_{\max}$, by setting $\tilde{x}(\tilde{t}_{\max}) = w$ which gives

$$\tilde{t}_{\max} = \frac{2\tilde{w}}{\tilde{v}_\ell \tan\theta}. \tag{47}$$

As in the previous section, we can solve for the unlatching time $\tilde{t}_\ell$ by setting $\tilde{f}(\tilde{t}_\ell) = \tilde{f}_{\text{spring}} = 1 - \tilde{x}(\tilde{t}_\ell)$

$$\tilde{t}_\ell = \min\left\{ \sqrt{\frac{4\tilde{w}}{\tilde{v}_\ell^2 \tan^2\theta} - 2\tilde{m}}\, ;\, \tilde{t}_{\max} \right\} \tag{48}$$

where the unlatching time $\tilde{t}_\ell = 0$ for $\tilde{m} > \tilde{m}_c$ with

$$\tilde{m}_c = \frac{2\tilde{w}}{\tilde{v}_\ell^2 \tan^2\theta}.$$

The mass reaches the end of the latch when $\tilde{t}_{\max} < \sqrt{\frac{4\tilde{w}}{\tilde{v}_\ell^2 \tan^2\theta} - 2\tilde{m}}$, which occurs when $\tilde{m} < (1-\tilde{w})\tilde{m}_c$.

Therefore, the unlatching time can be described in terms of the load mass by three different regimes: unlatching occurs after the full width of the latch ($\tilde{m} < (1-\tilde{w})\tilde{m}_c$), unlatching occurs along the edge of the latch ($(1-\tilde{w})\tilde{m}_c < \tilde{m} < \tilde{m}_c$), and unlatching occurs at $\tilde{t} = 0$ ($\tilde{m} > \tilde{m}_c$).

$$\tilde{t}_\ell = \begin{cases} \frac{2\tilde{w}}{\tilde{v}_\ell \tan\theta}, & \text{if } \tilde{m} < (1-\tilde{w})\tilde{m}_c \\ \sqrt{2\left(\tilde{m}_c - \tilde{m}\right)}, & \text{if } (1-\tilde{w})\tilde{m}_c < \tilde{m} < \tilde{m}_c \\ 0 & \text{if } \tilde{m} > \tilde{m}_c \end{cases} \tag{49}$$

The position after the unlatching phase is complete, is given by

$$\tilde{x}_\ell = \begin{cases} \tilde{w}, & \text{if } \tilde{m} < (1-\tilde{w})\tilde{m}_c \\ 1 - \frac{\tilde{m}}{\tilde{m}_c}, & \text{if } (1-\tilde{w})\tilde{m}_c < \tilde{m} < \tilde{m}_c \\ 0 & \text{if } \tilde{m} > \tilde{m}_c \end{cases} \tag{50}$$

During the unlatching, the velocity can be written in terms of position as

$$\tilde{v} = \tilde{v}_\ell \tan\theta \sqrt{\frac{\tilde{x}}{\tilde{w}}},$$

which means the velocity after the unlatching phase is complete, is given by

$$\tilde{v}_\ell = \tilde{v}_\ell \tan\theta \sqrt{\frac{\tilde{x}_\ell}{\tilde{w}}} = \sqrt{\frac{2\tilde{x}_\ell}{\tilde{m}_c}}, \tag{51}$$

After the unlatching, for $\tilde{t} > \tilde{t}_\ell$, the dynamics proceed identically to the process after the unlatching of the rounded latch (described in the previous section), according to Eqs.(35-42), but with $\tilde{t}_\ell, \tilde{x}_\ell, \tilde{v}_\ell$ defined by Eqs.(49), (50), and (51). This gives the take-off velocity, take-off time, and maximum power as

$$\tilde{v}_{\text{to}} = \begin{cases} \sqrt{\frac{(1-\tilde{w})^2}{\tilde{m}} + \tilde{v}_\ell^2 \tan^2\theta}, & \text{if } \tilde{m} < (1-\tilde{w})\tilde{m}_c \\ \sqrt{\frac{2}{\tilde{m}_c} - \frac{\tilde{m}}{\tilde{m}_c}}, & \text{if } (1-\tilde{w})\tilde{m}_c < \tilde{m} < \tilde{m}_c \\ \frac{1}{\sqrt{\tilde{m}}}, & \text{if } \tilde{m} > \tilde{m}_c \end{cases} \tag{52}$$

$$\tilde{t}_{\text{to}} = \begin{cases} \frac{\pi\sqrt{\tilde{m}}}{2} - \sqrt{\tilde{m}} \arctan\left(\frac{\sqrt{\tilde{m}}\tilde{v}_\ell \tan\theta}{1-\tilde{w}}\right) + \frac{2\tilde{w}}{\tilde{v}_\ell^2 \tan^2\theta}, & \text{if } \tilde{m} < (1-\tilde{w})\tilde{m}_c \\ \sqrt{\tilde{m}}\left[\frac{\pi}{2} - \arctan\left(\sqrt{2\left(\frac{\tilde{m}_c}{\tilde{m}} - 1\right)}\right) + \sqrt{2\left(\frac{\tilde{m}_c}{\tilde{m}} - 1\right)}\right] & \text{if } (1-\tilde{w})\tilde{m}_c < \tilde{m} < \tilde{m}_c \\ \frac{\pi\sqrt{\tilde{m}}}{2} & \text{if } \tilde{m} > \tilde{m}_c \end{cases} \tag{53}$$

$$\tilde{p}_{\max} = \frac{\sqrt{\tilde{m}}\tilde{v}_{\text{to}}^2}{2} \tag{54}$$

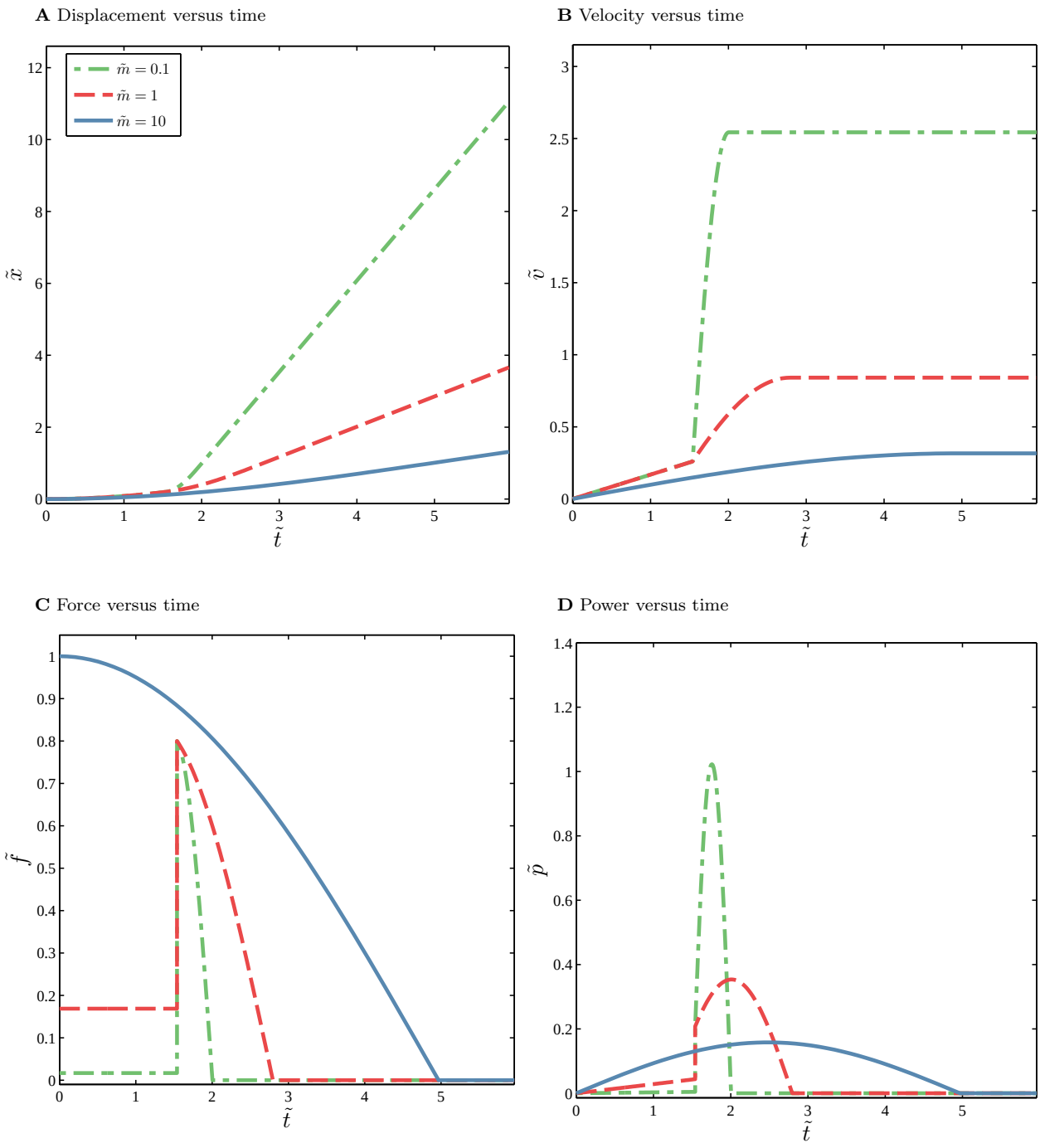

Figure S10: Dynamics of a system with a linear motor, ideal spring and parabolic latch shown for **A** displacement, **B** velocity, **C** force, and **D** power. The normalized width of the latch is set to $\tilde{w} = 0.2$, the final slope of the latch is $\theta = 60°$, and the velocity of the latch $\tilde{v}_\ell = 0.15$. The curves are plotted from Eqs. (43-46) for $\tilde{t} < \tilde{t}_\ell$ and Eqs. (35-38) for $\tilde{t} > \tilde{t}_\ell$.

Section S6 - Linear F-v motor + heavy spring + parabolic latch

In this section, the heavy spring from Section S3 will be combined with the parabolic latch from Section S5. As in the previous two sections, we need to consider when the latching force goes to zero. The inertia of the heavy spring adds an extra complication to this analysis, as the inertial force of the heavy spring needs to be accounted for. The approach we take here is to use an energy balance of the system, where the sum of the potential energy, total kinetic energy, and non-conservative work is constant:

$$\frac{1}{2}(1-\tilde{x})^2+\frac{1}{2}\left(\tilde{m}+\frac{\tilde{m}_s}{3}\right)\tilde{v}^2-\int_0^{\tilde{x}}\tilde{f}_{\text{latch}}(\tilde{x}')\,d\tilde{x}'=\text{constant} \tag{55}$$

The third term in Eq.(55) is the non-conservative work that the latch performs on the projectile. By taking $\frac{d}{d\tilde{x}}$ of the energy balance, this gives a force balance

$$\left(\tilde{m}+\frac{\tilde{m}_s}{3}\right)\tilde{a}(\tilde{x})=\tilde{f}_{\text{latch}}(\tilde{x})+(1-\tilde{x}), \tag{56}$$

where a is the instantaneous acceleration of the projectile. Equation (55) will be used to determine the latch release point $\tilde{f}_{\text{latch}}(\tilde{x}_\ell)=0$, and the dynamics after release. As in previous sections, we will first consider the dynamics before release, followed by the dynamics after release.

Before latch release

Before latch release, while the load mass is in contact with the latch, the dynamics proceed identically to Eqs.(43-46) outlined in Section S5. The addition of the heavy spring here only modifies the latch release time $\tilde{t}_\ell$, latch release point $\tilde{x}_\ell$, and latch release velocity $\tilde{v}_\ell$. To solve for $\tilde{t}_\ell$, we substitute Eq.(43) and Eq.(45) into Eq.(56), and set $\tilde{f}_{\text{latch}}=0$. Using steps that parallel Section S5 (identical steps but with $\tilde{m}\to\tilde{m}+\tilde{m}_s/3$), gives

$$\tilde{t}_\ell=\begin{cases}\frac{2\tilde{w}}{\tilde{v}_\ell\tan\theta}, & \text{if } \tilde{m}<\left(\tilde{m}_c-\frac{2\tilde{w}^2}{\tilde{v}_\ell^2\tan^2\theta}\right)\\ \sqrt{2\left(\tilde{m}_c-\tilde{m}\right)}, & \text{if } \left(\tilde{m}_c-\frac{2\tilde{w}^2}{\tilde{v}_\ell^2\tan^2\theta}\right)<\tilde{m}<\tilde{m}_c\\ 0 & \text{if } \tilde{m}>\tilde{m}_c\end{cases} \tag{57}$$

where the critical mass $\tilde{m}_c$ has changed due to the inertia of the heavy spring and is given by

$$\tilde{m}_c=\frac{2\tilde{w}}{\tilde{v}_\ell^2\tan^2\theta}-\frac{\tilde{m}_s}{3}. \tag{58}$$

The position after the unlatching phase is complete, is given by

$$\tilde{x}_\ell=\begin{cases}\tilde{w}, & \text{if } \tilde{m}<\left(\tilde{m}_c-\frac{2\tilde{w}^2}{\tilde{v}_\ell^2\tan^2\theta}\right)\\ \frac{\tilde{v}_\ell^2\tan^2\theta}{2\tilde{w}}\left(\tilde{m}_c-\tilde{m}\right), & \text{if } \left(\tilde{m}_c-\frac{2\tilde{w}^2}{\tilde{v}_\ell^2\tan^2\theta}\right)<\tilde{m}<\tilde{m}_c\\ 0 & \text{if } \tilde{m}>\tilde{m}_c\end{cases} \tag{59}$$

As in Section S5, during the unlatching, the velocity can be written in terms of position as

$$\tilde{v}=\tilde{v}_\ell\tan\theta\sqrt{\frac{\tilde{x}}{\tilde{w}}},$$

which means the velocity after the unlatching phase is complete, is given by

$$\tilde{v}_\ell=\tilde{v}_\ell\tan\theta\sqrt{\frac{\tilde{x}_\ell}{\tilde{w}}}. \tag{60}$$

After latch release

The dynamics after the latch releases proceeds as in Section S3; however, the initial conditions are altered. From Eq.(56) with $\tilde{f}_{\text{latch}}$ set to zero, and setting the maximum velocity equal to the take-off velocity, the motion of the load mass is described by a simple harmonic motion:

$$\tilde{x}(\tilde{t}) = 1 - \tilde{v}_{\text{to}}\sqrt{\tilde{m} + \frac{\tilde{m}_s}{3}}\cos\left(\frac{\tilde{t}}{\sqrt{\tilde{m} + \frac{\tilde{m}_s}{3}}} + \tilde{\phi}\right) \tag{61}$$

$$\tilde{v}(\tilde{t}) = \tilde{v}_{\text{to}}\sin\left(\frac{\tilde{t}}{\sqrt{\tilde{m} + \frac{\tilde{m}_s}{3}}} + \tilde{\phi}\right) \tag{62}$$

$$\tilde{f}(\tilde{t}) = \frac{\tilde{m}\tilde{v}_{\text{to}}}{\sqrt{\tilde{m} + \frac{\tilde{m}_s}{3}}}\cos\left(\frac{\tilde{t}}{\sqrt{\tilde{m} + \frac{\tilde{m}_s}{3}}} + \tilde{\phi}\right) \tag{63}$$

$$\tilde{p}(\tilde{t}) = \frac{\tilde{m}\tilde{v}_{\text{to}}^2}{2\sqrt{\tilde{m} + \frac{\tilde{m}_s}{3}}}\sin\left(2\left(\frac{\tilde{t}}{\sqrt{\tilde{m} + \frac{\tilde{m}_s}{3}}} + \tilde{\phi}\right)\right), \tag{64}$$

with the non-dimensional take-off velocity $\tilde{v}_{\text{to}}$ and phase $\tilde{\phi}$ given by the initial conditions $\tilde{x}_\ell$, $\tilde{v}_\ell$, $\tilde{t}_\ell$ as

$$\tilde{v}_{\text{to}} = \sqrt{\frac{(1-\tilde{x}_\ell)^2}{\tilde{m} + \frac{\tilde{m}_s}{3}} + \tilde{v}_\ell^2} \tag{65}$$

$$\tilde{\phi} = \arctan\left(\frac{\sqrt{\tilde{m} + \frac{\tilde{m}_s}{3}}\tilde{v}_\ell}{1-\tilde{x}_\ell}\right) - \frac{\tilde{t}_\ell}{\sqrt{\tilde{m} + \frac{\tilde{m}_s}{3}}} \tag{66}$$

The take-off time occurs at the maximum of $\tilde{v}(\tilde{t})$, when $\frac{\tilde{t}_{\text{to}}}{\sqrt{\tilde{m}+\frac{\tilde{m}_s}{3}}} + \tilde{\phi} = \frac{\pi}{2}$,

$$\tilde{t}_{\text{to}} = \frac{\pi\sqrt{\tilde{m} + \frac{\tilde{m}_s}{3}}}{2} - \sqrt{\tilde{m} + \frac{\tilde{m}_s}{3}}\arctan\left(\frac{\sqrt{\tilde{m} + \frac{\tilde{m}_s}{3}}\tilde{v}_\ell}{1-\tilde{x}_\ell}\right) + \tilde{t}_\ell. \tag{67}$$

The force after unlatching can be written in terms of $\tilde{x}$ and $\tilde{m}$ as

$$\tilde{f} = \frac{\tilde{m}}{\tilde{m} + \frac{\tilde{m}_s}{3}}(1-\tilde{x}). \tag{68}$$

To determine the force-displacement-velocity trade-off after unlatching $\tilde{f}(\tilde{x}, \tilde{v})$ requires some extra steps compared to previous sections. First, invoking the Pythagorean trigonometric identity on $\tilde{x}(\tilde{t})$ and $\tilde{v}(\tilde{t})$ yields

$$\frac{1}{\tilde{m} + \frac{\tilde{m}_s}{3}} = \frac{\tilde{v}_{\text{to}}^2 - \tilde{v}^2}{(1-\tilde{x})^2} \tag{69}$$

and

$$\tilde{m} = \frac{(1-\tilde{x})^2}{\tilde{v}_{\text{to}}^2 - \tilde{v}^2} - \frac{\tilde{m}_s}{3}. \tag{70}$$

These two relations allow Eq.(68) to be written in terms of $\tilde{x}$ and $\tilde{v}_{\text{to}}$

$$\tilde{f} = \left(1 - \frac{\tilde{m}_s(\tilde{v}_{\text{to}}^2 - \tilde{v}^2)}{3(1-\tilde{x})^2}\right)(1-\tilde{x}), \tag{71}$$

where $\tilde{v}_{\text{to}}$ depends on $\tilde{x}_\ell$ through Eq.(65), which in turn depends on $\tilde{m}$. To eliminate the implicit $\tilde{m}$ dependence in Eq.(71), we note that all three cases for $\tilde{x}_\ell$ of the parabolic latch from Eq.(59) have the form

$$\tilde{x}_\ell = a + b\tilde{m}, \tag{72}$$

where the constants a and b are given by

$$a = \begin{cases} \tilde{w}, & \text{if } \tilde{m} < \left(\tilde{m}_c - \frac{2\tilde{w}^2}{\tilde{v}_\ell^2 \tan^2\theta}\right) \\ 1 + b\frac{\tilde{m}_s}{3}, & \text{if } \left(\tilde{m}_c - \frac{2\tilde{w}^2}{\tilde{v}_\ell^2 \tan^2\theta}\right) < \tilde{m} < \tilde{m}_c \\ 0 & \text{if } \tilde{m} > \tilde{m}_c \end{cases} \tag{73}$$

$$b = \begin{cases} 0, & \text{if } \tilde{m} < \left(\tilde{m}_c - \frac{2\tilde{w}^2}{\tilde{v}_\ell^2 \tan^2\theta}\right) \\ \frac{-\tilde{v}_\ell^2 \tan^2\theta}{2\tilde{w}}, & \text{if } \left(\tilde{m}_c - \frac{2\tilde{w}^2}{\tilde{v}_\ell^2 \tan^2\theta}\right) < \tilde{m} < \tilde{m}_c \\ 0 & \text{if } \tilde{m} > \tilde{m}_c. \end{cases} \tag{74}$$

Substituting $\tilde{x}_\ell = a + b\tilde{m}$ into the expression for $\tilde{v}_{\text{to}}$ in Eq.(65), making use of the relationship between $\tilde{v}_\ell$ and $\tilde{x}_\ell$ for the parabolic latch [Eq.(60)] and the expression for $\tilde{m}$ in Eq.(70) gives a quadratic equation in $\tilde{v}_{\text{to}}^2 - \tilde{v}^2$:

$$\begin{aligned} \left(\tilde{v}_{\text{to}}^2 - \tilde{v}^2\right)^2 \left[(1 - a + b\frac{\tilde{m}_s}{3})^2 - (1-\tilde{x})^2\right] + \\ \left(\tilde{v}_{\text{to}}^2 - \tilde{v}^2\right) \left[\left(\frac{\tilde{v}_\ell^2 \tan^2\theta}{\tilde{w}}(a - b\frac{\tilde{m}_s}{3}) - \tilde{v}^2 - 2b(1 - a + b\frac{\tilde{m}_s}{3})\right)(1-\tilde{x})^2\right] + \\ \left[\left(b^2 + \frac{b\tilde{v}_\ell^2 \tan^2\theta}{\tilde{w}}\right)(1-\tilde{x})^4\right] = 0. \end{aligned} \tag{75}$$

The solution to this equation can be found by splitting the mass into the three cases. **Case 1:** $\tilde{m} < \tilde{m}_c - \frac{2\tilde{w}^2}{\tilde{v}_\ell^2 \tan^2\theta}$ In this case, the mass reaches the end of the latch before release, with $a = \tilde{w}$ and $b = 0$. This results in

$$\tilde{v}_{\text{to}}^2 - \tilde{v}^2 = \frac{(\tilde{v}^2 - \tilde{v}_\ell^2 \tan^2\theta)(1-\tilde{x})^2}{(1-\tilde{w})^2 - (1-\tilde{x})^2}, \tag{76}$$

which when substituted into Eq.(71) gives

$$\tilde{f}(\tilde{x}, \tilde{v}) = \left(1 - \frac{\tilde{m}_s(\tilde{v}^2 - \tilde{v}_\ell^2 \tan^2\theta)}{3\left((1-\tilde{w})^2 - (1-\tilde{x})^2\right)}\right)(1-\tilde{x}). \tag{77}$$

Case 2: $\tilde{m}_c - \frac{2\tilde{w}^2}{\tilde{v}_\ell^2 \tan^2\theta} < \tilde{m} < \tilde{m}_c$ In this case, the mass slips off the latch before it reaches the end of the latch width, with $a = 1 + \frac{\tilde{m}_s}{3}b$ and $b = \frac{-\tilde{v}_\ell^2 \tan^2\theta}{2\tilde{w}}$. Terms in Eq.(75) simplify because here $a - b\frac{\tilde{m}_s}{3} = 1$, which gives

$$\left(\tilde{v}_{\text{to}}^2 - \tilde{v}^2\right)^2 + \left(\tilde{v}_{\text{to}}^2 - \tilde{v}^2\right)\left(2b + \tilde{v}^2\right) + b^2(1-\tilde{x})^2 = 0. \tag{78}$$

The quadratic formula can then be used to solve for $\tilde{v}_{\text{to}}^2 - \tilde{v}^2$, which gives

$$\tilde{v}_{\text{to}}^2 - \tilde{v}^2 = \frac{1}{2}\left[-\left(\tilde{v}^2 + 2b\right) - \sqrt{\left(\tilde{v}^2 + 2b\right)^2 - 4b^2(1-\tilde{x})^2}\right]. \tag{79}$$

This gives the force as a function of displacement and velocity as

$$\tilde{f}(\tilde{x}, \tilde{v}) = (1-\tilde{x})\left(1 - \frac{\tilde{m}_s\left[-\left(\tilde{v}^2 + 2b\right) - \sqrt{\left(\tilde{v}^2 + 2b\right)^2 - 4b^2(1-\tilde{x})^2}\right]}{6(1-\tilde{x})^2}\right). \tag{80}$$

Case 3: $\tilde{m} > \tilde{m}_c$ In this case, the load mass is so heavy that the latch slips off instantly with $\tilde{x}_\ell = \tilde{v}_\ell = 0$. This corresponds to $a = b = 0$, which gives

$$\tilde{v}_{\text{to}}^2 - \tilde{v}^2 = \frac{\tilde{v}^2(1-\tilde{x})^2}{1-(1-\tilde{x})^2}, \tag{81}$$

and

$$\tilde{f}(\tilde{x}, \tilde{v}) = \left(1 - \frac{\tilde{m}_s \tilde{v}^2}{3(1-(1-\tilde{x})^2)}\right)(1-\tilde{x}), \tag{82}$$

which is equivalent to the heavy spring + ideal latch in Eq.(26) of Section S3.

The results of these three cases are summarized in Fig. S2F and Fig. S11

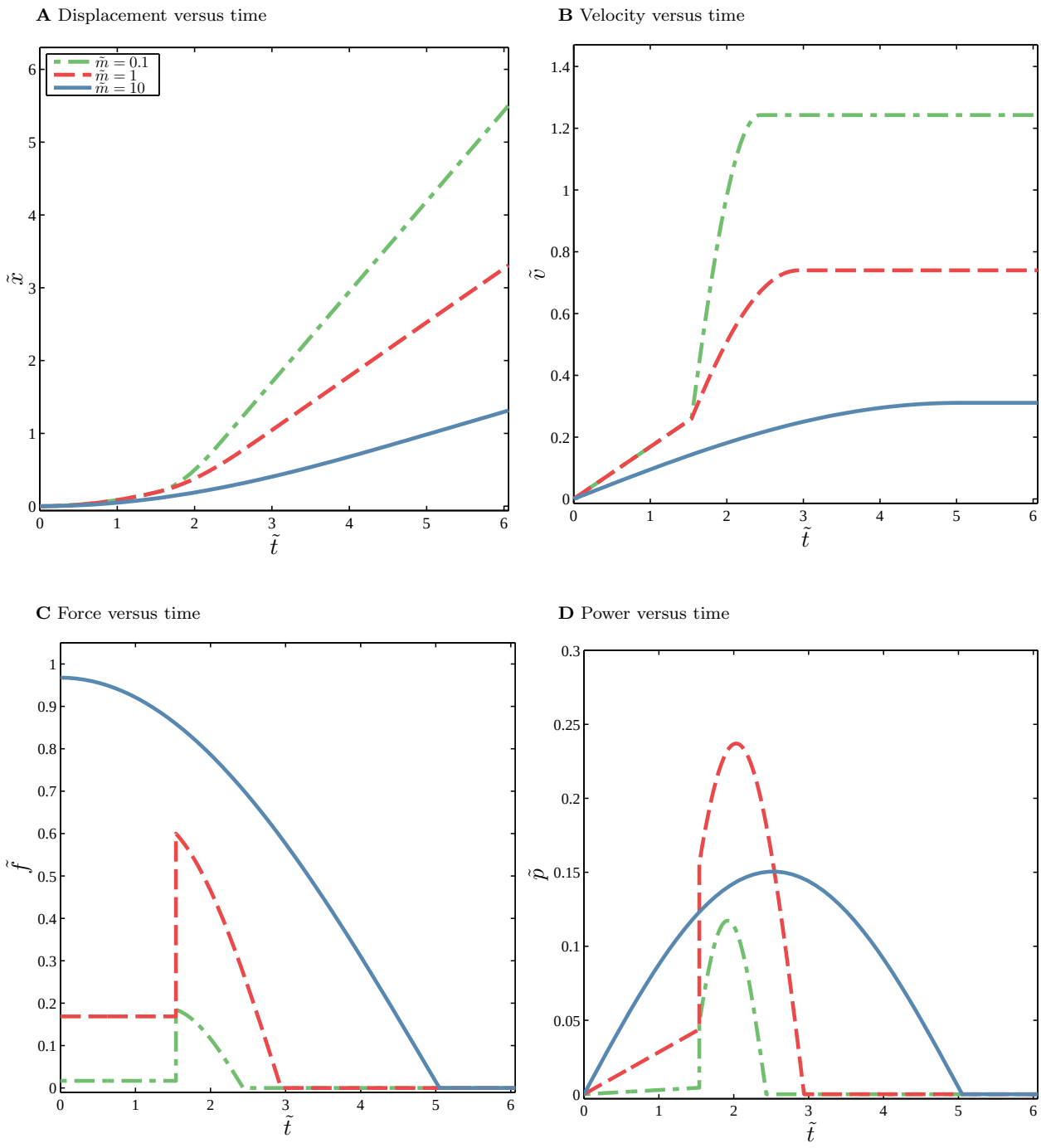

Figure S11: Dynamics of a system with a linear motor, heavy spring and parabolic latch shown for **A** displacement, **B** velocity, **C** force, and **D** power. The normalized width of the latch is set to $\tilde{w} = 0.2$, the final slope of the latch is $\theta = 60°$, and the velocity of the latch $\tilde{v}_\ell = 0.15$. The mass of the spring is set to $\tilde{m}_s = 1$. The curves are plotted from Eqs. (43-46) for $\tilde{t} < \tilde{t}_\ell$ and Eqs. (61-64) for $\tilde{t} > \tilde{t}_\ell$.

Section S7 - When is spring-driven motion beneficial?

In this section, we prove the proposition for a motor-driven motion compared to spring-driven motion from a motor/spring/latch system:

There is a potential benefit for spring-driven motion if and only if the motor has a sufficient F-v trade-off.

Specifically, we let $F_m(x, v)$ define the motor force-displacement-velocity behavior, with a range-of-motion of the motor d such that $F_m(x, v) = 0$ for all $x > d$. Let $F_s(x)$ define the force-displacement loading and unloading behavior of the spring. Since the spring is loaded by the motor, this means that the spring force is less than that of the motor loading it at zero velocity, $F_s(x) < F_m(x, v = 0)$. To prove the theorem, first suppose that the motor has no F-v trade-off, such that: $F_m(x, v > 0) \geq F_m(x, v = 0)$ for all x and v.

The kinetic energy of a project undergoing motor-driven motion, KE_m, is given by
$\mathrm{KE}_m = \int_0^d F_m(x, v)\, dx \geq \int_0^d F_m(x, v = 0)\, dx > \int_0^d F_s(x)\, dx = \mathrm{KE}_s$,
and therefore $\mathrm{KE}_m > \mathrm{KE}_s$, where KE_s is the kinetic energy of the projectile undergoing spring-driven motion. Therefore, if there is no F-v trade-off of the motor, there is no benefit to using a spring-driven system.

Second, suppose now that the motor does have a sufficient F-v trade-off of the motor such that there exists a $v_{\max}$ such that $F_m(x, v) = 0$ for all $v > v_{\max}$. Then $\mathrm{KE}_m \leq 1/2 m v_{\max}^2$, where m is the mass of the projectile. Since KE_s is independent of m, and $\lim_{m \to 0} 1/2 m v_{\max}^2 = 0$, then there exists an m such that:
$\mathrm{KE}_m < \mathrm{KE}_s$.
Therefore, with a sufficient F-v trade-off of the motor, then spring-driven motion can be potentially be beneficial.

Section S8 - Load mass with a rounded edge

In the previous sections, we considered the edges of the load mass to be perfectly sharp, and tested the effect of rounding the latch geometry. Here we consider the effect of rounded the edges of the load mass by examining the simple case of parabolic shaped edges as in Fig. S12.

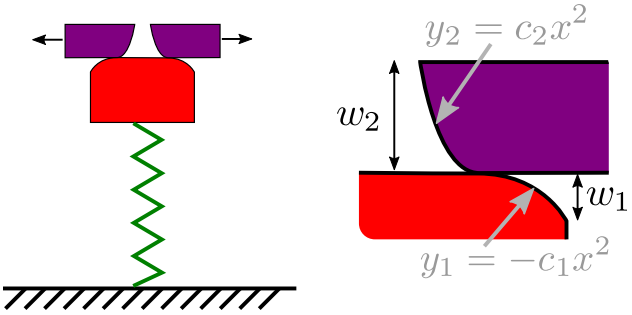

Figure S12: Schematic showing parabolic shaped latches in contact with a mass with a rounded corner also in the shape of a parabola.

If the center-of-mass motion of the latch is given by $x_{\rm lch}(t)$, and, as a result, the load mass moves along the vertical trajectory $y_{\rm ld}(t)$ while in contact with the latch, then the surface of the two faces can be described by

$$y_1(x) = -c_1x^2 + y_{\rm ld}(t)$$
$$y_2(x) = c_2(x - x_{\rm lch}(t))^2$$

We would like to determine the displacement of the load mass $y_{\rm ld}(t)$, as a function of the displacement of the latch $x_{\rm lch}(t)$. To do this, we find the position of minimum distance between the latch and load surfaces $x_{\rm min}$, and solve for the load mass displacement that gives $y_1(x_{\rm min}) = y_2(x_{\rm min})$. The condition for finding the minimum distance between the two surfaces is

$$\frac{d}{dx}(y_2 - y_1)|_{x=x_{\rm min}} = 0,$$

which gives

$$x_{\rm min} = \frac{c_2}{c_1 + c_2}x_{\rm lch}(t).$$

Using this expression for $x_{\rm min}$ in $y_1(x_{\rm min}) = y_2(x_{\rm min})$ gives

$$y_{\rm ld}(t) = \left[c_2\left(\frac{c_2}{c_1 + c_2} - 1\right)^2 + \frac{c_1c_2^2}{(c_1 + c_2)^2}\right]x_{\rm lch}(t)^2,$$

which is valid for $y_{\rm ld} < (w_1 + w_2)$.

By letting $w = w_1 + w_2$ and

$$c = c_2\left(\frac{c_2}{c_1 + c_2} - 1\right)^2 + \frac{c_1c_2^2}{(c_1 + c_2)^2}$$

this gives the displacement of the load in terms of the displacement of the latch in an equivalent form as the case where the load mass has sharp edges:

$$y_{\rm ld} = cx_{\rm lch}(t)^2,$$

for $y_{\rm ld} < w$. Having rounded edges load mass leads to a geometric factor given by c, but otherwise the dynamics are the same as for a load mass with sharp edges.

Table S3. **Dataset of the mass, speed and acceleration from the biological literature.** For jumping organisms, the mass reflects the whole body. For organisms that move projectiles or body parts, the reported mass is of the moving structure.

Phylum	Class	Order	Family	Genus	species	common name	mass (kg)	speed (m/s)	acceleration (m/s^2)	Citation
Anthophyta	Dicotyledoneae	Cornales	Cornaceae	*Cornus*	*canadensis*	Bunchberry dogwood	4.0×10^{-7}	7.5	2.4×10^{4}	(108,109)
Arthropoda	Arachnida	Araneae	Ctenidae	*Cupiennius*	*salei*	Central American hunting spider/wandering spider	1.26×10^{-3}	1.26	5.51×10^{1}	(131)
Arthropoda	Crustacea	Stomatopoda	Gonodactylidae	*Gonodactylus*	*smithii*	mantis shrimp	9.24×10^{-3}		2.5×10^{5}	(112)
Arthropoda	Crustacea	Stomatopoda	Odontodactylidae	*Odontodactylus*	*scyllarus*	mantis shrimp	1.78×10^{-3}		$1. \times 10^{5}$	(112)
Arthropoda	Insecta	Blattodea	Ectobiidae	*Saltoblattella*	*montistabularis*	jumping cockroach/leaproach	1.4×10^{-5}	2.1	2.2×10^{2}	(132)
Arthropoda	Insecta	Coleoptera	Chrysomelidae	*Altica*	*lythri*	flea beetle	1.22×10^{-5}	7.5×10^{-1}	1×10^{2}	(133)
Arthropoda	Insecta	Coleoptera	Chrysomelidae	*Aphthona*	*atrocaerulea*	flea beetle	6.4×10^{-7}	1.7	1.13×10^{3}	(133)
Arthropoda	Insecta	Coleoptera	Chrysomelidae	*Crepidodera*	*aurata*	willow flea beetle	2.7×10^{-6}	8.3×10^{-1}	2.5×10^{2}	(133)
Arthropoda	Insecta	Coleoptera	Chrysomelidae	*Longitarsus*	*gracilis*	flea beetle	2.75×10^{-6}	2.7	1.93×10^{3}	(133)
Arthropoda	Insecta	Coleoptera	Chrysomelidae	*Podagrica*	*fuscicornis*	mallow flea beetle	5.94×10^{-6}	7.2×10^{-1}	1.2×10^{2}	(133)
Arthropoda	Insecta	Coleoptera	Chrysomelidae	*Psylliodes*	*affinis*	flea beetle/leaf beetle	1.28×10^{-6}	2.93	2.66×10^{3}	(133)
Arthropoda	Insecta	Coleoptera	Chrysomelidae	*Psylliodes*	*dulcamarae*	flea beetle	6.11×10^{-6}	2.34	1.1×10^{3}	(133)
Arthropoda	Insecta	Coleoptera	Elateridae	*Athous*	*haemorrhoidalis*	click beetle/skipjack	3.01×10^{-5}	2.8	3.8×10^{3}	(134)
Arthropoda	Insecta	Coleoptera	Elateridae	*Lanelater*	*judaicus*	click-beetle	$2. \times 10^{-4}$	1.75		(135)
Arthropoda	Insecta	Diptera	Dolichopodidae	*Hydrophorus*	*alboflorens*	long-legged fly	4.7×10^{-6}	1.64	1.414×10^{2}	(136)
Arthropoda	Insecta	Diptera	Drosophilidae	*Drosophila*	*virilis*	fruit fly	1.23×10^{-6}	$4. \times 10^{-1}$	1.2×10^{2}	(137)
Arthropoda	Insecta	Hemiptera	Aphalaridae	*Psyllopsis*	*fraxini*	jumping plant louse	1.2×10^{-6}	1.9	2.34×10^{3}	(111)
Arthropoda	Insecta	Hemiptera	Aphrophoridae	*Aphrophora*	*alni*	European Alder Spittle Bug/froghopper species	2.83×10^{-5}	3.4	2.267×10^{3}	(99)

Arthropoda	Insecta	Hemiptera	Aphrophoridae	*Lepyronia*	*coleoptrata*	froghopper/spittlebug	1.76×10^{-5}	4.6	3.067×10^{3}	(99)
Arthropoda	Insecta	Hemiptera	Aphrophoridae	*Neophilaenus*	*exclamationis*	froghopper	3.2×10^{-6}	4.2	4.2×10^{3}	(99)
Arthropoda	Insecta	Hemiptera	Aphrophoridae	*Philaenus*	*spumarius*	meadow froghopper/meadow spittlebug	1.23×10^{-5}	4.7	5.4×10^{3}	(99)
Arthropoda	Insecta	Hemiptera	Cercopidae	*Cercopis*	*vulnerata*	Black-and-red froghopper	3.29×10^{-5}	3.8	2.533×10^{3}	(99)
Arthropoda	Insecta	Hemiptera	Cicadellidae	*Aphrodes*	*makarovi, bicinctus*	leafhopper, girdled leafhopper	1.84×10^{-5}	2.9	1.055×10^{3}	(138)
Arthropoda	Insecta	Hemiptera	Cicadellidae	*Cephalelus*	*angustatus*	short-legged leafhoppers	9.2×10^{-6}	2	$1. \times 10^{3}$	(50)
Arthropoda	Insecta	Hemiptera	Cicadellidae	*Cicadella*	*viridis*	green leafhopper	1.5×10^{-5}	8.8×10^{-1}	1.52×10^{2}	(84)
Arthropoda	Insecta	Hemiptera	Cicadellidae	*Empoasca*	*vitis*	green leafhopper	8.6×10^{-7}	1.6	$4. \times 10^{2}$	(138)
Arthropoda	Insecta	Hemiptera	Cicadellidae	*Graphocephala*	*fennahi*	Rhododendron leafhopper	1.3×10^{-5}	1.85	4.11×10^{2}	(138)
Arthropoda	Insecta	Hemiptera	Cicadellidae	*Iassus*	*lanio*	leafhopper (nymphs)	$4. \times 10^{-6}$	2	$8. \times 10^{2}$	(138)
Arthropoda	Insecta	Hemiptera	Cicadellidae	*Pauroeurymela*	*amplicincta*	Australian gum treehopper	2.3×10^{-5}	3.8	2.71×10^{3}	(139)
Arthropoda	Insecta	Hemiptera	Cicadellidae	*Ulopa*	*reticulata*	short-legged leafhoppers	2.1×10^{-6}	2.3	2.3×10^{3}	(50)
Arthropoda	Insecta	Hemiptera	Dictyopharidae	*Dictyophara*	*europaea*	dictyopharid planthoppers	2.29×10^{-5}	4.4	2.29×10^{3}	(140)
Arthropoda	Insecta	Hemiptera	Dictyopharidae	*Engela*	*minuta*	dictyopharid planthoppers	5.7×10^{-6}	5.8	4.83×10^{3}	(140)
Arthropoda	Insecta	Hemiptera	Dictyopharidae	*Raphiophora*	*vitrea*	dictyopharid planthoppers	1.96×10^{-5}	4	3.33×10^{3}	(140)
Arthropoda	Insecta	Hemiptera	Dictyopharidae	*Thanatodictya*	*praeferrata*	dictyopharid planthoppers	8.1×10^{-6}	4.4	3.67×10^{3}	(140)
Arthropoda	Insecta	Hemiptera	Flatidae	*Colgar*	*peracutum*	planthopper	1.93×10^{-5}	3.2	1.8×10^{3}	(141)
Arthropoda	Insecta	Hemiptera	Flatidae	*Metcalfa*	*pruinosa*	Citrus flatid planthopper	8.3×10^{-6}	2.9	1.71×10^{3}	(141)
Arthropoda	Insecta	Hemiptera	Flatidae	*Siphanta*	*acuta*	planthopper/torpedo bug	1.37×10^{-5}	2.8	1.96×10^{3}	(141)
Arthropoda	Insecta	Hemiptera	Issidae	*Issus*	*coleoptratus*	planthopper	2.15×10^{-5}	5.5	7.051×10^{3}	(142)
Arthropoda	Insecta	Hemiptera	Membracidae	*Campylenchia*	*latipes*	treehopper	6.6×10^{-6}	2.3	1.67×10^{3}	(143)

Arthropoda	Insecta	Hemiptera	Membracidae	*Carynota*	*marmorata*	treehopper	2.5×10^{-5}	2.5	9.6×10^{2}	(143)
Arthropoda	Insecta	Hemiptera	Membracidae	*Ceresa*	*basalis*	treehopper	2.85×10^{-5}	2	5.9×10^{2}	(143)
Arthropoda	Insecta	Hemiptera	Membracidae	*Entylia*	*carinata*	treehopper	4.8×10^{-6}	2.7	2.45×10^{3}	(143)
Arthropoda	Insecta	Hemiptera	Membracidae	*Publilia*	*concava*	treehopper	3.8×10^{-6}	2.6	2.36×10^{3}	(143)
Arthropoda	Insecta	Hemiptera	Membracidae	*Sextius*	*spp*	treehopper	1.87×10^{-5}	2.1	1.22×10^{3}	(143)
Arthropoda	Insecta	Hemiptera	Membracidae	*Stictocephala*	*bisonia*	Buffalo treehopper	2.68×10^{-5}	2.7	7.7×10^{2}	(143)
Arthropoda	Insecta	Hemiptera	Membracidae	*Telamona*	*compacta (a.k.a. ampelopsidis)*	treehopper	4.12×10^{-5}	1.9	5.6×10^{2}	(143)
Arthropoda	Insecta	Hemiptera	Peloridiidae	*Hackeriella*	*veitchi*	Gondwanan relict insect	1.28×10^{-6}	1.5	9.66×10^{2}	(144)
Arthropoda	Insecta	Hemiptera	Psyllidae	*Cacopsylla*	*peregrina*	jumping plant louse	$7. \times 10^{-7}$	2.5	6.25×10^{3}	(111)
Arthropoda	Insecta	Hemiptera	Psyllidae	*Psylla*	*alni*	jumping plant louse	2.8×10^{-6}	2.7	2.7×10^{3}	(111)
Arthropoda	Insecta	Hemiptera	Saldidae	*Saldula*	*saltatoria*	common shorebug/hemipteran shore bug	2.1×10^{-6}	1.8	5.29×10^{2}	(145)
Arthropoda	Insecta	Hymenoptera	Formicidae	*Odontomachus*	*bauri*	trap-jaw ant (escape jump)	1.21×10^{-5}	2.9×10^{-1}	8.624×10^{3}	(110)
Arthropoda	Insecta	Hymenoptera	Formicidae	*Odontomachus*	*bauri*	trap-jaw ant (bouncer defense)	1.21×10^{-5}	2.3	1.298×10^{4}	(110)
Arthropoda	Insecta	Hymenoptera	Formicidae	*Odontomachus*	*bauri*	trap-jaw ant (mandible closure)	1.45×10^{-7}	6.43×10^{1}	1×10^{6}	(110)
Arthropoda	Insecta	Hymenoptera	Formicidae	*Odontomachus*	*brunneus*	trap-jaw ant mandibles	$7. \times 10^{-8}$	6.65×10^{1}	1.59×10^{6}	(146)
Arthropoda	Insecta	Hymenoptera	Formicidae	*Odontomachus*	*cephalotes*	trap-jaw ant mandibles	1.62×10^{-7}	4.83×10^{1}	1.15×10^{6}	(146)
Arthropoda	Insecta	Hymenoptera	Formicidae	*Odontomachus*	*chelifer*	trap-jaw ant mandibles	3.1×10^{-7}	5.31×10^{1}	8.73×10^{5}	(146)
Arthropoda	Insecta	Hymenoptera	Formicidae	*Odontomachus*	*clarus*	trap-jaw ant mandibles	9.5×10^{-8}	6.53×10^{1}	1.74×10^{6}	(146)
Arthropoda	Insecta	Hymenoptera	Formicidae	*Odontomachus*	*erythrocephalus*	trap-jaw ant mandibles	1.44×10^{-7}	6.43×10^{1}	1.57×10^{6}	(146)
Arthropoda	Insecta	Hymenoptera	Formicidae	*Odontomachus*	*haematodus*	trap-jaw ant mandibles	5.6×10^{-8}	5.68×10^{1}	1.45×10^{6}	(146)
Arthropoda	Insecta	Hymenoptera	Formicidae	*Odontomachus*	*ruginodis*	trap-jaw ant mandibles	5.2×10^{-8}	$5. \times 10^{1}$	1.47×10^{6}	(146)

Arthropoda	Insecta	Isoptera	Termitidae	*Termes*	*panamaensis*	termite soldier mandibles	2.82×10^{-8}	6.7×10^{1}		(147)
Arthropoda	Insecta	Lepidoptera	Crambidae	*Crambus*	*pascuella*	grass veneer	1.19×10^{-5}	$9. \times 10^{-1}$	3.7×10^{1}	(148)
Arthropoda	Insecta	Lepidoptera	Crambidae	*Udea*	*olivalis*	olive pearl	1.91×10^{-5}	1	4.3×10^{1}	(148)
Arthropoda	Insecta	Lepidoptera	Geometridae	*Camptogramma*	*bilineata*	yellow shell	1.46×10^{-5}	1	6.1×10^{1}	(148)
Arthropoda	Insecta	Lepidoptera	Geometridae	*Idaea*	*seriata*	small dusty wave	4.6×10^{-6}	$7. \times 10^{-1}$	8.8×10^{1}	(148)
Arthropoda	Insecta	Lepidoptera	Geometridae	*Xanthorhoe*	*fluctuata*	garden carpet	1.74×10^{-5}	1	5.7×10^{1}	(148)
Arthropoda	Insecta	Lepidoptera	Noctuidae	*Apamea*	*lithoxylaea*	light arches	2.21×10^{-4}	$8. \times 10^{-1}$	2.9×10^{1}	(148)
Arthropoda	Insecta	Lepidoptera	Oecophoridae	*Hofmannophila*	*pseudospretella*	brown hous x 10-moth	5.4×10^{-6}	1.2	7.1×10^{1}	(148)
Arthropoda	Insecta	Lepidoptera	Tortricidae	*Acleris*	*sparsana*	ashy button	6.3×10^{-6}	$8. \times 10^{-1}$	$4. \times 10^{1}$	(148)
Arthropoda	Insecta	Lepidoptera	Tortricidae	*Epiphyas*	*postvittana*	light brown apple	7.7×10^{-6}	1	9.2×10^{1}	(148)
Arthropoda	Insecta	Lepidoptera	Xyloryctidae	*Thyrocopa*	*apatela*	flightless hawaiian grasshopper moth/Haleakala flightless moth	3.35×10^{-5}	9.4×10^{-1}		(149)
Arthropoda	Insecta	Lepidoptera	Xyloryctidae	*Thyrocopa*	*kikaelekea*	flightless hawaiian grasshopper moth	3.33×10^{-5}	8.1×10^{-1}		(149)
Arthropoda	Insecta	Mecoptera	Boreidae	*Boreus*	*hyemalis*	snow flea/snow scorpion flies	2.9×10^{-6}	1	1.61×10^{2}	(150)
Arthropoda	Insecta	Neuroptera	Chrysopidae	*Chrysoperla*	*carnea*	green lacewing	$9. \times 10^{-6}$	1	5.4×10^{1}	(151)
Arthropoda	Insecta	Neuroptera	Hemerobiidae	*Micromus*	*variegatus*	brown lacewings	3.6×10^{-6}	$6. \times 10^{-1}$	6.2×10^{1}	(151)
Arthropoda	Insecta	Odonata	Aeshnidae	*Aeshna*	*nigroflava and juncea*	dragonfly larvae	$7. \times 10^{-5}$	1		(152)
Arthropoda	Insecta	Orthoptera	Acrididae	*Schistocerca*	*gregaria*	desert locust/gregarious desert locust	1.8×10^{-3}	3.2	1.8×10^{2}	(116)
Arthropoda	Insecta	Orthoptera	Proscopiidae	*Prosarthria*	*teretrirostris*	false stick insect	2.8×10^{-4}	2.5	1.65×10^{2}	(153)
Arthropoda	Insecta	Orthoptera	Tettigoniidae	*Conocephalus*	*dorsalis*	short-winged conehead/short-winged meadow Katydid	1.3×10^{-4}	1		(154)
Arthropoda	Insecta	Orthoptera	Tettigoniidae	*Meconema*	*thalassinum*	oak bush-cricket/drumming katydid	1.74×10^{-4}	1.4		(154)
Arthropoda	Insecta	Orthoptera	Tettigoniidae	*Pholidoptera*	*griseoaptera*	dark bush-cricket	6.02×10^{-4}	2.12	1.438×10^{2}	(154)

Arthropoda	Insecta	Orthoptera	Tridactylidae	*Xya*	*capensis var. capensis*	pygmy mole cricket (jumping on ground)	8.3×10^{-6}	5.4	$3. \times 10^{3}$	(98)
Arthropoda	Insecta	Orthoptera	Tridactylidae	*Xya*	*capensis var. capensis*	pygmy mole crickets (jumping on water)	9.2×10^{-6}	2.2	1.57×10^{3}	(100)
Arthropoda	Insecta	Phasmatodea	Timematidae	*Timema*	*chumash*	wingless stick insect	4.75×10^{-5}	$9. \times 10^{-1}$	7.5×10^{1}	(50)
Arthropoda	Insecta	Phasmida	Phylliidae	*Sipyloidea*	*sp.*	Thailand winged stick insect/Sipyloidea sp. 'Thailand 8'	1.64×10^{-4}	$8. \times 10^{-1}$	$1. \times 10^{1}$	(155)
Arthropoda	Insecta	Siphonaptera	Pulicidae	*Spilopsyllus*	*cuniculi*	rabbit flea	4.5×10^{-7}	1.2	1.33×10^{3}	(156)
Arthropoda	Insecta	Trichoptera	Leptoceridae	*Mystacides*	*azureus*	silverhorn/caddis fly	3.9×10^{-6}	$9. \times 10^{-1}$	5.1×10^{1}	(157)
Arthropoda	Insecta	Trichoptera	Limnephilidae	*Limnephilus*	*marmoratus*	cinnamon sedge/caddis fly	3.81×10^{-5}	1.1	5.7×10^{1}	(157)
Arthropoda	Insecta	Trichoptera	Molannidae	*Molanna*	*angustata*	caddis fly	1.13×10^{-5}	1.1	6.4×10^{1}	(157)
Ascomycota	Pezizomycetes	Pezizales	Ascobolaceae	*Ascobolus*	*immersus*	Ascomycota fungi	8.8×10^{-10}		1.8×10^{6}	(158,159)
Athropoda	Insecta	Siphonaptera	Pulicidae	*Archaeopsylla*	*erinacei*	hedgehog flea	$7. \times 10^{-7}$	1.9	1.6×10^{3}	(49)
Basidiomycota	Agaricomycetes	Auriculariales	Auriculariaceae	*Auricularia*	*auricula*	jelly fungus	3.7×10^{-13}	1.62	1.177×10^{5}	(107,160)
Basidiomycota	Tremellomycetes	Cystofilobasidiales	Cystofilobasidiaceae	*Itersonilia*	*perplexans*	Basidiomycota fungi	1.5×10^{-12}	6.7×10^{-1}	2.499×10^{5}	(161)
Chordata	Amphibia	Anura	Myobatrachidae	*Limnodynastes*	*peronii*	striped marsh frog	2.9×10^{-3}		1.08×10^{2}	(162)
Chordata	Aves	Falconiformes	Falconidae	*Falco*	*rusticolus*	gyrfalcon/gerfalcon	1.02	5.8×10^{1}	1.2×10^{1}	(163)
Chordata	Mammalia	Carnivora	Felidae	*Acinonyx*	*jubatus*	cheetah	5.3×10^{1}	2.59×10^{1}	1.3×10^{1}	(164)
Chordata	Reptilia	Squamata	Chamaeleonidae	*Rhampholeon*	*spinosus*	Chameleon	8.7×10^{-5}	5.3	2.6×10^{3}	(114,115)
Cnidaria	Hydrozoa	Anthomedusae	Hydridae	*Hydra*	*spp*	White hydra, Brown hydra	2.3×10^{-12}	1.86×10^{1}	5.41×10^{7}	(103)
Nematoda	Secernentea	Rhabditida	Steinernematidae	*Steinernema*	*carpocapsae*	entomopathogenic nematode	2.18×10^{-10}	1.134	1.609×10^{3}	(165)

References

1. P. Aerts, Vertical jumping in *Galago senegalensis*: The quest for an obligate mechanical power amplifier. *Philos. Trans. R. Soc. Lond. B Biol. Sci.* **353**, 1607–1620 (1998). doi:10.1098/rstb.1998.0313

2. M. M. Peplowski, R. L. Marsh, Work and power output in the hindlimb muscles of Cuban tree frogs *Osteopilus septentrionalis* during jumping. *J. Exp. Biol.* **200**, 2861–2870 (1997). Medline

3. M. Burrows, Biomechanics: Froghopper insects leap to new heights. *Nature* **424**, 509 (2003). doi:10.1038/424509a Medline

4. O. Barth, Harmonic piezodrive—miniaturized servo motor. *Mechatronics* **10**, 545–554 (2000). doi:10.1016/S0957-4158(99)00062-8

5. L. C. Rome, S. L. Lindstedt, The quest for speed: Muscles built for high-frequency contractions. *Physiology* **13**, 261–268 (1998). doi:10.1152/physiologyonline.1998.13.6.261 Medline

6. T. J. Roberts, E. Azizi, Flexible mechanisms: The diverse roles of biological springs in vertebrate movement. *J. Exp. Biol.* **214**, 353–361 (2011). doi:10.1242/jeb.038588 Medline

7. S. N. Patek, D. M. Dudek, M. V. Rosario, From bouncy legs to poisoned arrows: Elastic movements in invertebrates. *J. Exp. Biol.* **214**, 1973–1980 (2011). doi:10.1242/jeb.038596 Medline

8. W. Gronenberg, Fast actions in small animals: Springs and click mechanisms. *J. Comp. Physiol. A Neuroethol. Sens. Neural Behav. Physiol.* **178**, 727–734 (1996). doi:10.1007/BF00225821

9. R. McN. Alexander, H. C. Bennet-Clark, Storage of elastic strain energy in muscle and other tissues. *Nature* **265**, 114–117 (1977). doi:10.1038/265114a0 Medline

10. R. M. Alexander, *Elastic Mechanisms in Animal Movement* (Cambridge Univ. Press, 1988).

11. D. P. Ferris, M. Louie, C. T. Farley, Running in the real world: Adjusting leg stiffness for different surfaces. *Proc. R. Soc. London Ser. B* **265**, 989–994 (1998). doi:10.1098/rspb.1998.0388 Medline

12. A. Galantis, R. C. Woledge, The theoretical limits to the power output of a muscle-tendon complex with inertial and gravitational loads. *Proc. R. Soc. London Ser. B* **270**, 1493–1498 (2003). doi:10.1098/rspb.2003.2403 Medline

13. S. N. Patek, The most powerful movements in biology. *Am. Sci.* **103**, 330–337 (2015). doi:10.1511/2015.116.330

14. D. Cofer, G. Cymbalyuk, W. J. Heitler, D. H. Edwards, Neuromechanical simulation of the locust jump. *J. Exp. Biol.* **213**, 1060–1068 (2010). doi:10.1242/jeb.034678 Medline

15. W. Gronenberg, B. Ehmer, The mandible mechanism of the ant genus Anochetus (Hymenoptera, Formicidae) and the possible evolution of trap-jaws. *Zoology* **99**, 153–162 (1996).

16. M. M. Blanco, S. N. Patek, Muscle trade-offs in a power-amplified prey capture system. *Evolution* **68**, 1399–1414 (2014). doi:10.1111/evo.12365 Medline

17. X. Noblin, N. O. Rojas, J. Westbrook, C. Llorens, M. Argentina, J. Dumais, The fern sporangium: A unique catapult. *Science* **335**, 1322 (2012). doi:10.1126/science.1215985 Medline

18. O. Vincent, C. Weisskopf, S. Poppinga, T. Masselter, T. Speck, M. Joyeux, C. Quilliet, P. Marmottant, Ultra-fast underwater suction traps. *Proc. R. Soc. London Ser. B* **278**, 2909–2914 (2011). doi:10.1098/rspb.2010.2292 Medline

19. J. M. Skotheim, L. Mahadevan, Physical limits and design principles for plant and fungal movements. *Science* **308**, 1308–1310 (2005). doi:10.1126/science.1107976 Medline

20. Y. Forterre, J. M. Skotheim, J. Dumais, L. Mahadevan, How the Venus flytrap snaps. *Nature* **433**, 421–425 (2005). doi:10.1038/nature03185 Medline

21. M. Kovac, M. Fuchs, A. Guignard, J.-C. Zufferey, D. Floreano, *in IEEE International Conference on Robotics and Automation* (IEEE, 2008), pp. 373–378.

22. F. Li, W. Liu, X. Fu, G. Bonsignori, U. Scarfogliero, C. Stefanini, P. Dario, Jumping like an insect: Design and dynamic optimization of a jumping mini robot based on bio-mimetic inspiration. *Mechatronics* **22**, 167–176 (2012). doi:10.1016/j.mechatronics.2012.01.001

23. J. Zhao, in *IEEE International Conference on Robotics and Automation* (IEEE, 2011), pp. 4614–4619.

24. B. G. A. Lambrecht, A. D. Horchler, R. D. Quinn, in *IEEE International Conference on Robotics and Automation* (IEEE, 2005), pp. 1240–1245.

25. S. A. Stoeter, P. E. Rybski, M. Gini, N. Papanikolopoulos, in *IEEE Int. Conf. Intell. Robot. Syst.* **1**, 721–726 (2002).

26. N. Fukamachi, H. Mochiyama, in *IEEE International Conference on Advanced Intelligent Mechatronics* (IEEE, 2015) pp. 1102–1107.

27. J. Burdick, P. Fiorini, Minimalist jumping robots for celestial exploration. *Int. J. Robot. Res.* **22**, 653–674 (2003). doi:10.1177/02783649030227013

28. M. Kaneko, M. Higashimori, in *Automation Congress* (IEEE, 2004), pp. 117–122.

29. A. M. Johnson, D. E. Koditschek, in *IEEE International Conference on Robotics and Automation* (IEEE, 2013), pp. 2568–2575.

30. A. Namiki, Y. Imai, M. Ishikawa, M. Kaneko, in *IEEE/RSJ International Conference on Intelligent Robots and Systems* (IEEE, 2003), pp. 2666–2671.

31. V. Zaitsev, O. Gvirsman, U. Ben Hanan, A. Weiss, A. Ayali, G. Kosa, A locust-inspired miniature jumping robot. *Bioinspir. Biomim.* **10**, 066012 (2015). doi:10.1088/1748-3190/10/6/066012 Medline

32. J. S. Koh, E. Yang, G.-P. Jung, S.-P. Jung, J. H. Son, S.-I. Lee, P. G. Jablonski, R. J. Wood, H.-Y. Kim, K.-J. Cho, Jumping on water: Surface tension-dominated jumping of water striders and robotic insects. *Science* **349**, 517–521 (2015). doi:10.1126/science.aab1637 Medline

33. J. S. Koh, S. Jung, R. J. Wood, K. Cho, in *IEEE/RSJ International Conference on Intelligent Robots and Systems* (IEEE, 2013), pp. 3796–3801.

34. S. W. Kim, J.-S. Koh, J.-G. Lee, J. Ryu, M. Cho, K.-J. Cho, Flytrap-inspired robot using structurally integrated actuation based on bistability and a developable surface. *Bioinspir. Biomim.* **9**, 036004 (2014). doi:10.1088/1748-3182/9/3/036004 Medline

35. W. Lindsay, D. Teasdale, V. Milanovic, K. Pister, C. Fernandez-Pello, in *IEEE International Conference on Micro Electro Mechanical Systems* (IEEE, 2001), pp. 606–610.

36. S. J. Apperson, A. V. Bezmelnitsyn, R. Thiruvengadathan, K. Gangopadhyay, S. Gangopadhyay, W. A. Balas, P. E. Anderson, S. M. Nicolich, Characterization of nanothermite material for solid-fuel microthruster applications. *J. Propuls. Power* **25**, 1086–1091 (2009). doi:10.2514/1.43206

37. W. A. Churaman, L. J. Currano, C. J. Morris, J. E. Rajkowski, S. Bergbreiter, The first launch of an autonomous thrust-driven microrobot using nanoporous energetic silicon. *J. Microelectromech. Syst.* **21**, 198–205 (2012). doi:10.1109/JMEMS.2011.2174414

38. R. Niiyama, A. Nagakubo, in *IEEE International Conference on Robotics and Automation* (IEEE, 2007), pp. 2546–2551.

39. Boston dynamics Inc., Sandflea, https://www.bostondynamics.com/sandflea.

40. H. Tsukagoshi, M. Sasaki, A. Kitagawa, T. Tanaka, in *IEEE International Conference on Robotics and Automation* (IEEE, 2005), pp. 1276–1283.

41. F. E. Zajac, Muscle and tendon: Properties, models, scaling, and application to biomechanics and motor control. *Crit. Rev. Biomed. Eng.* **17**, 359–411 (1989).

42. T. J. Roberts, R. L. Marsh, Probing the limits to muscle-powered accelerations: Lessons from jumping bullfrogs. *J. Exp. Biol.* **206**, 2567–2580 (2003). doi:10.1242/jeb.00452 Medline

43. R. F. Ker, Dynamic tensile properties of the plantaris tendon of sheep (*Ovis aries*). *J. Exp. Biol.* **93**, 283–302 (1981). Medline

44. R. F. Ker, R. McN. Alexander, M. B. Bennett, Why are mammalian tendons so thick? *J. Zool.* **216**, 309–324 (1988). doi:10.1111/j.1469-7998.1988.tb02432.x

45. J. F. V. Vincent, U. G. K. Wegst, Design and mechanical properties of insect cuticle. *Arthropod Struct. Dev.* **33**, 187–199 (2004). doi:10.1016/j.asd.2004.05.006 Medline

46. M. V. Rosario, G. P. Sutton, S. N. Patek, G. S. Sawicki, Muscle-spring dynamics in time-limited, elastic movements. *Proc. R. Soc. London Ser. B* **283**, 20161561 (2016). doi:10.1098/rspb.2016.1561 Medline

47. M. Burrows, S. R. Shaw, G. P. Sutton, Resilin and chitinous cuticle form a composite structure for energy storage in jumping by froghopper insects. *BMC Biol.* **6**, 41 (2008). doi:10.1186/1741-7007-6-41 Medline

48. M. Burrows, G. P. Sutton, Locusts use a composite of resilin and hard cuticle as an energy store for jumping and kicking. *J. Exp. Biol.* **215**, 3501–3512 (2012). doi:10.1242/jeb.071993 Medline

49. G. P. Sutton, M. Burrows, Biomechanics of jumping in the flea. *J. Exp. Biol.* **214**, 836–847 (2011). doi:10.1242/jeb.052399 Medline

50. S. N. Patek, M. V. Rosario, J. R. A. Taylor, Comparative spring mechanics in mantis shrimp. *J. Exp. Biol.* **216**, 1317–1329 (2013). doi:10.1242/jeb.078998 Medline

51. J. Gosline, M. Lillie, E. Carrington, P. Guerette, C. Ortlepp, K. Savage, Elastic proteins: Biological roles and mechanical properties. *Philos. Trans. R. Soc. Lond. B Biol. Sci.* **357**, 121–132 (2002). doi:10.1098/rstb.2001.1022 Medline

52. D. Raabe, C. Sachs, P. Romano, The crustacean exoskeleton as an example of a structurally and mechanically graded biological nanocomposite material. *Acta Mater.* **53**, 4281–4292 (2005). doi:10.1016/j.actamat.2005.05.027

53. J. F. V. Vincent, Arthropod cuticle: A natural composite shell system. *Compos., Part A Appl. Sci. Manuf.* **33**, 1311–1315 (2002). doi:10.1016/S1359-835X(02)00167-7

54. D. Klocke, H. Schmitz, Water as a major modulator of the mechanical properties of insect cuticle. *Acta Biomater.* **7**, 2935–2942 (2011). doi:10.1016/j.actbio.2011.04.004 Medline

55. M. V. Rosario, S. N. Patek, Multilevel analysis of elastic morphology: The mantis shrimp's spring. *J. Morphol.* **276**, 1123–1135 (2015). doi:10.1002/jmor.20398 Medline

56. D. W. Haldane, M. M. Plecnik, J. K. Yim, R. S. Fearing, Robotic vertical jumping agility via series-elastic power modulation. *Sci. Robot.* **1**, eaag2048 (2016). doi:10.1126/scirobotics.aag2048

57. D. Rollinson, S. Ford, B. Brown, H. Choset, in *Proceedings of the ASME 2013 Dynamic Systems and Control Conference*. (ASME, 2013) p. v001T08A002.

58. B. Hopkinson, A method of measuring the pressure produced in the detonation of high explosives or by the impact of bullets. *Phil. Trans. R. Soc. A* **213**, 437–456 (1914). doi:10.1098/rsta.1914.0010

59. K. W. Hillier, H. Kolsky, An investigation of the dynamic elastic properties of some high polymers. *Proc. Phys. Soc. London. Sect. B* **62**, 111–121 (1949). doi:10.1088/0370-1301/62/2/304

60. B. Justusson, M. Pankow, C. Heinrich, M. Rudolph, A. M. Waas, Use of a shock tube to determine the bi-axial yield of an aluminum alloy under high rates. *Int. J. Impact Eng.* **58**, 55–65 (2013). doi:10.1016/j.ijimpeng.2013.01.012

61. J. Yi, M. C. Boyce, G. F. Lee, E. Balizer, Large deformation rate-dependent stress–strain behavior of polyurea and polyurethanes. *Polymer* **47**, 319–329 (2006). doi:10.1016/j.polymer.2005.10.107

62. G. H. Staab, A. Gilat, A direct-tension split Hopkinson bar for high strain-rate testing. *Exp. Mech.* **31**, 232–235 (1991). doi:10.1007/BF02326065

63. M. Hudspeth, B. Claus, S. Dubelman, J. Black, A. Mondal, N. Parab, C. Funnell, F. Hai, M. L. Qi, K. Fezzaa, S. N. Luo, W. Chen, High speed synchrotron x-ray phase contrast imaging of dynamic material response to split Hopkinson bar loading. *Rev. Sci. Instrum.* **84**, 025102 (2013). doi:10.1063/1.4789780 Medline

64. A. D. Mulliken, M. C. Boyce, Mechanics of the rate-dependent elastic–plastic deformation of glassy polymers from low to high strain rates. *Int. J. Solids Struct.* **43**, 1331–1356 (2006). doi:10.1016/j.ijsolstr.2005.04.016

65. C. C. Chen, J. Y. Chueh, H. Tseng, H. M. Huang, S. Y. Lee, Preparation and characterization of biodegradable PLA polymeric blends. *Biomaterials* **24**, 1167–1173 (2003). doi:10.1016/S0142-9612(02)00466-0 Medline

66. B. Wetzel, P. Rosso, F. Haupert, K. Friedrich, Epoxy nanocomposites: Fracture and toughening mechanisms. *Eng. Fract. Mech.* **73**, 2375–2398 (2006). doi:10.1016/j.engfracmech.2006.05.018

67. C. R. Siviour, J. L. Jordan, High strain rate mechanics of polymers: A review. *J. Dyn. Behav. Mat.* **2**, 15–32 (2016). doi:10.1007/s40870-016-0052-8

68. R. B. Bogoslovov, C. M. Roland, Viscoelastic effects on the free retraction of rubber. *J. Appl. Phys.* **102**, 063531 (2007). doi:10.1063/1.2784018

69. P. H. Mott J. N. Twigg, C. Michael Roland, K. E. Nugent, T. E. Hogan, C. G. Robertson, Comparison of the transient stress-strain response of rubber to its linear dynamic behavior. *J. Polym. Sci., B, Polym. Phys.* **49**, 1195–1202 (2011). doi:10.1002/polb.22292

70. C. C. Lawrence, G. J. Lake, A. G. Thomas, The deformation and fracture of balloons. *Int. J. Non-linear Mech.* **68**, 59–65 (2015). doi:10.1016/j.ijnonlinmec.2014.08.009

71. J. G. Niemczura, "On the response of rubbers at high strain rates" (Tech. Rep., Sandia National Laboratories, Albuquerque, NM, and Livermore, CA 2010).

72. R. Vermorel, N. Vandenberghe, E. Villermaux, Rubber band recoil. *Proc. R. Soc. A* **463**, 641–658 (2007). doi:10.1098/rspa.2006.1781

73. L. B. Tunnicliffe, A. G. Thomas, J. J. C. Busfield, The free retraction of natural rubber: A momentum-based model. *Polym. Test.* **47**, 36–41 (2015). doi:10.1016/j.polymertesting.2015.07.012

74. C. M. Roland, Mechanical behavior of rubber at high strain rates. *Rubber Chem. Technol.* **79**, 429–459 (2006). doi:10.5254/1.3547945

75. K. Kagaya, S. N. Patek, Feed-forward motor control of ultrafast, ballistic movements. *J. Exp. Biol.* **219**, 319–333 (2016). doi:10.1242/jeb.130518 Medline

76. A. Sakes, M. van der Wiel, P. W. J. Henselmans, J. L. van Leeuwen, D. Dodou, P. Breedveld, Shooting mechanisms in nature: A systematic review. *PLOS ONE* **11**, e0158277 (2016). doi:10.1371/journal.pone.0158277 Medline

77. M. S. Rodgers, J. J. Allen, K. D. Meeks, B. D. Jensen, S. L. Miller, in *Proceedings of SPIE* (1999), pp. 212–222.

78. R. E. Fischell, L. Wilson, Spacecraft application of subliming materials. *J. Spacecr. Rockets* **2**, 376–379 (1965). doi:10.2514/3.28187

79. W. Gronenberg, J. Tautz, B. Hölldobler, Fast trap jaws and giant neurons in the ant odontomachus. *Science* **262**, 561–563 (1993). doi:10.1126/science.262.5133.561 Medline

80. Y. Forterre, Slow, fast and furious: Understanding the physics of plant movements. *J. Exp. Bot.* **64**, 4745–4760 (2013). doi:10.1093/jxb/ert230 Medline

81. R. Ritzmann, Snapping behavior of the shrimp *Alpheus californiensis*. *Science* **181**, 459–460 (1973). doi:10.1126/science.181.4098.459 Medline

82. F. Liu, R. L. Chavez, S. N. Patek, A. Pringle, J. J. Feng, C. H. Chen, Asymmetric drop coalescence launches fungal ballistospores with directionality. *J. R. Soc. Interface* **14**, 20170083 (2017). doi:10.1098/rsif.2017.0083 Medline

83. W. J. Heitler, The locust jump. *J. Comp. Physiol.* **89**, 93–104 (1974). doi:10.1007/BF00696166

84. G. Bonsignori, C. Stefanini, U. Scarfogliero, S. Mintchev, G. Benelli, P. Dario, The green leafhopper, *Cicadella viridis* (Hemiptera, Auchenorrhyncha, Cicadellidae), jumps with near-constant acceleration. *J. Exp. Biol.* **216**, 1270–1279 (2013). doi:10.1242/jeb.076083 Medline

85. F. C. Moon, *The Machines of Leonardo Da Vinci and Franz Reuleaux: Kinematics of Machines from the Renaissance to the 20th Century* (Springer Science & Business Media, 2007).

86. J. M. Keep, Animal trap, Patent, U.S. Patent Office (1879).

87. M. M. Muñoz, P. S. L. Anderson, S. N. Patek, Mechanical sensitivity and the dynamics of evolutionary rate shifts in biomechanical systems. *Proc. R. Soc. London Ser. B* **284**, 20162325 (2017). doi:10.1098/rspb.2016.2325 Medline

88. T. Claverie, E. Chan, S. N. Patek, Modularity and scaling in fast movements: Power amplification in mantis shrimp. *Evolution* **65**, 443–461 (2011). doi:10.1111/j.1558-5646.2010.01133.x Medline

89. T. Claverie, S. N. Patek, Modularity and rates of evolutionary change in a power-amplified prey capture system. *Evolution* **67**, 3191–3207 (2013). doi:10.1111/evo.12185 Medline

90. P. S. L. Anderson, D. C. Smith, S. N. Patek, Competing influences on morphological modularity in biomechanical systems: A case study in mantis shrimp. *Evol. Dev.* **18**, 171–181 (2016). doi:10.1111/ede.12190 Medline

91. P. S. L. Anderson, S. N. Patek, Mechanical sensitivity reveals evolutionary dynamics of mechanical systems. *Proc. R. Soc. London Ser. B* **282**, 20143088 (2015). doi:10.1098/rspb.2014.3088 Medline

92. J. Aguilar, A. Lesov, K. Wiesenfeld, D. I. Goldman, Lift-off dynamics in a simple jumping robot. *Phys. Rev. Lett.* **109**, 174301 (2012). doi:10.1103/PhysRevLett.109.174301 Medline

93. N. W. Bartlett, M. T. Tolley, J. T. B. Overvelde, J. C. Weaver, B. Mosadegh, K. Bertoldi, G. M. Whitesides, R. J. Wood, A 3D-printed, functionally graded soft robot powered by combustion. *Science* **349**, 161–165 (2015). doi:10.1126/science.aab0129 Medline

94. S. Vogel, *Glimpses of Creatures in Their Physical Worlds* (Princeton Univ. Press, Princeton 2009).

95. S. Vogel, Living in a physical world III. Getting up to speed. *J. Biosci.* **30**, 303–312 (2005). doi:10.1007/BF02703667 Medline

96. S. Vogel, Living in a physical world II. The bio-ballistics of small projectiles. *J. Biosci.* **30**, 167–175 (2005). doi:10.1007/BF02703696 Medline

97. H. C. Bennet-Clark, E. C. Lucey, The jump of the flea: A study of the energetics and a model of the mechanism. *J. Exp. Biol.* **47**, 59–67 (1967). Medline

98. M. Burrows, M. D. Picker, Jumping mechanisms and performance of pygmy mole crickets (Orthoptera, Tridactylidae). *J. Exp. Biol.* **213**, 2386–2398 (2010). doi:10.1242/jeb.042192 Medline

99. M. Burrows, Jumping performance of froghopper insects. *J. Exp. Biol.* **209**, 4607–4621 (2006). doi:10.1242/jeb.02539 Medline

100. M. Burrows, G. P. Sutton, Pygmy mole crickets jump from water. *Curr. Biol.* **22**, R990–R991 (2012). doi:10.1016/j.cub.2012.10.045 Medline

101. S. E. Bergbreiter, thesis, University of California, Berkeley (2007).

102. L. G. Leal, *Advanced Transport Phenomena: Fluid Mechanics and Convective Transport Processes*, vol. 7 (Cambridge Univ. Press, 2007).

103. T. Nüchter, M. Benoit, U. Engel, S. Ozbek, T. W. Holstein, Nanosecond-scale kinetics of nematocyst discharge. *Curr. Biol.* **16**, R316–R318 (2006). doi:10.1016/j.cub.2006.03.089 Medline

104. E. Purcell, Life at low Reynolds number. *Am. J. Phys.* **45**, 3–11 (1977). doi:10.1119/1.10903

105. S. Spagnolie, *Complex Fluids in Biological Systems: Experiment, Theory, and Computation* (Springer, New York 2014).

106. A. W. Koch, T. W. Holstein, C. Mala, E. Kurz, J. Engel, C. N. David, Spinalin, a new glycine- and histidine-rich protein in spines of Hydra nematocysts. *J. Cell Sci.* **111**, 1545–1554 (1998). Medline

107. A. Pringle, S. N. Patek, M. Fischer, J. Stolze, N. P. Money, The captured launch of a ballistospore. *Mycologia* **97**, 866–871 (2005). doi:10.1080/15572536.2006.11832777 Medline

108. J. Edwards, D. Whitaker, S. Klionsky, M. J. Laskowski, Botany: A record-breaking pollen catapult. *Nature* **435**, 164 (2005). doi:10.1038/435164a Medline

109. D. L. Whitaker, L. A. Webster, J. Edwards, The biomechanics of *Cornus canadensis* stamens are ideal for catapulting pollen vertically. *Funct. Ecol.* **21**, 219–225 (2007). doi:10.1111/j.1365-2435.2007.01249.x

110. S. N. Patek, J. E. Baio, B. L. Fisher, A. V. Suarez, Multifunctionality and mechanical origins: Ballistic jaw propulsion in trap-jaw ants. *Proc. Natl. Acad. Sci. U.S.A.* **103**, 12787–12792 (2006). doi:10.1073/pnas.0604290103 Medline

111. M. Burrows, Jumping mechanisms in jumping plant lice (Hemiptera, Sternorrhyncha, Psyllidae). *J. Exp. Biol.* **215**, 3612–3621 (2012). doi:10.1242/jeb.074682 Medline

112. M. J. McHenry, P. S. L. Anderson, S. Van Wassenbergh, D. G. Matthews, A. P. Summers, S. N. Patek, The comparative hydrodynamics of rapid rotation by predatory appendages. *J. Exp. Biol.* **219**, 3399–3411 (2016). doi:10.1242/jeb.140590 Medline

113. R. S. James, R. S. Wilson, Explosive jumping: Extreme morphological and physiological specializations of Australian rocket frogs (*Litoria nasuta*). *Physiol. Biochem. Zool.* **81**, 176–185 (2008). doi:10.1086/525290 Medline

114. C. V. Anderson, T. Sheridan, S. M. Deban, Scaling of the ballistic tongue apparatus in chameleons. *J. Morphol.* **273**, 1214–1226 (2012). doi:10.1002/jmor.20053 Medline

115. C. V. Anderson, Off like a shot: Scaling of ballistic tongue projection reveals extremely high performance in small chameleons. *Sci. Rep.* **6**, 18625 (2016). doi:10.1038/srep18625 Medline

116. H. C. Bennet-Clark, The energetics of the jump of the locust *Schistocerca gregaria*. *J. Exp. Biol.* **63**, 53–83 (1975). Medline

117. A. P. Gerratt, S. Bergbreiter, Incorporating compliant elastomers for jumping locomotion in microrobots. *Smart Mater. Struct.* **22**, 014010 (2013). doi:10.1088/0964-1726/22/1/014010

118. A. Debray, Manipulators inspired by the tongue of the chameleon. *Bioinspir. Biomim.* **6**, 026002 (2011). doi:10.1088/1748-3182/6/2/026002 Medline

119. J. S. Koh, S. P. Jung, M. Noh, S. W. Kim, K. J. Cho, in *IEEE International Conference on Robotics and Automation* (IEEE, 2013), pp. 26–31.

120. J. Zhao, J. Xu, B. Gao, N. Xi, F. J. Cintron, M. W. Mutka, L. Xiao, MSU Jumper: A single-motor-actuated miniature steerable jumping robot. *IEEE Trans. Robot.* **29**, 602–614 (2013). doi:10.1109/TRO.2013.2249371

121. P. Weiss, Hop... Hop... Hopbots! *Sci. News* **159**, 88–91 (2001). doi:10.2307/3981566

122. J. German, Sandia-developed intelligent software agents challenge electronic intruders. *Sandia Lab News* **52**(10), LN05-19-00 (19 May 2000); http://www.sandia.gov/LabNews/LN05-19-00/software_story.html

123. S. N. Patek, B. N. Nowroozi, J. E. Baio, R. L. Caldwell, A. P. Summers, Linkage mechanics and power amplification of the mantis shrimp's strike. *J. Exp. Biol.* **210**, 3677–3688 (2007). doi:10.1242/jeb.006486 Medline

124. M. Versluis, B. Schmitz, A. von der Heydt, D. Lohse, How snapping shrimp snap: Through cavitating bubbles. *Science* **289**, 2114–2117 (2000). doi:10.1126/science.289.5487.2114 Medline

125. H. C. Astley, T. J. Roberts, Evidence for a vertebrate catapult: Elastic energy storage in the plantaris tendon during frog jumping. *Biol. Lett.* **8**, 386–389 (2012). doi:10.1098/rsbl.2011.0982 Medline

126. H. C. Astley, T. J. Roberts, The mechanics of elastic loading and recoil in anuran jumping. *J. Exp. Biol.* **217**, 4372–4378 (2014). doi:10.1242/jeb.110296 Medline

127. X. Noblin, S. Yang, J. Dumais, Surface tension propulsion of fungal spores. *J. Exp. Biol.* **212**, 2835–2843 (2009). doi:10.1242/jeb.029975 Medline

128. L. Mahadevan, P. Matsudaira, Motility powered by supramolecular springs and ratchets. *Science* **288**, 95–99 (2000). doi:10.1126/science.288.5463.95 Medline

129. J. H. de Groot, J. L. van Leeuwen, Evidence for an elastic projection mechanism in the chameleon tongue. *Proc. R. Soc. London Ser. B* **271**, 761–770 (2004). doi:10.1098/rspb.2003.2637 Medline

130. U. K. Müller, S. Kranenbarg, Power at the tip of the tongue. *Science* **304**, 217–219 (2004). doi:10.1126/science.1097894 Medline

131. T. Weihmann, M. Karner, R. J. Full, R. Blickhan, Jumping kinematics in the wandering spider Cupiennius salei. *J. Comp. Physiol. A Neuroethol. Sens. Neural Behav. Physiol.* **196**, 421–438 (2010). doi:10.1007/s00359-010-0527-3 Medline

132. M. Picker, J. F. Colville, M. Burrows, A cockroach that jumps. *Biol. Lett.* **8**, 390–392 (2012). doi:10.1098/rsbl.2011.1022 Medline

133. J. Brackenbury, R. Wang, Ballistics and visual targeting in flea-beetles (Alticinae). *J. Exp. Biol.* **198**, 1931–1942 (1995). Medline

134. M. E. G. Evans, The jump of the click beetle (Coleoptera, Elateridae)-a preliminary study. *J. Zool.* **167**, 319–336 (1972). doi:10.1111/j.1469-7998.1972.tb03115.x

135. G. Ribak, D. Weihs, Jumping without using legs: The jump of the click-beetles (Elateridae) is morphologically constrained. *PLOS ONE* **6**, e20871 (2011). doi:10.1371/journal.pone.0020871 Medline

136. M. Burrows, Jumping from the surface of water by the long-legged fly *Hydrophorus* (Diptera, Dolichopodidae). *J. Exp. Biol.* **216**, 1973–1981 (2013). doi:10.1242/jeb.083683 Medline

137. M.-W. Chen, M. Sun, *Lixue Xuebao* **30**, 495–506 (2014).

138. M. Burrows, Kinematics of jumping in leafhopper insects (Hemiptera, Auchenorrhyncha, Cicadellidae). *J. Exp. Biol.* **210**, 3579–3589 (2007). doi:10.1242/jeb.009092 Medline

139. M. Burrows, Jumping mechanisms in gum treehopper insects (Hemiptera, Eurymelinae). *J. Exp. Biol.* **216**, 2682–2690 (2013). doi:10.1242/jeb.085266 Medline

140. M. Burrows, Jumping mechanisms in dictyopharid planthoppers (Hemiptera, Dicytyopharidae). *J. Exp. Biol.* **217**, 402–413 (2014). doi:10.1242/jeb.093476 Medline

141. M. Burrows, Jumping mechanisms in flatid planthoppers (Hemiptera, Flatidae). *J. Exp. Biol.* **217**, 2590–2600 (2014). doi:10.1242/jeb.105429 Medline

142. M. Burrows, Jumping performance of planthoppers (Hemiptera, Issidae). *J. Exp. Biol.* **212**, 2844–2855 (2009). doi:10.1242/jeb.032326 Medline

143. M. Burrows, Jumping mechanisms of treehopper insects (Hemiptera, Auchenorrhyncha, Membracidae). *J. Exp. Biol.* **216**, 788–799 (2013). doi:10.1242/jeb.078741 Medline

144. M. Burrows, V. Hartung, H. Hoch, Jumping behaviour in a Gondwanan relict insect (Hemiptera: Coleorrhyncha: Peloridiidae). *J. Exp. Biol.* **210**, 3311–3318 (2007). doi:10.1242/jeb.007914 Medline

145. M. Burrows, Jumping strategies and performance in shore bugs (Hemiptera, Heteroptera, Saldidae). *J. Exp. Biol.* **212**, 106–115 (2009). doi:10.1242/jeb.024448 Medline

146. J. C. Spagna, A. I. Vakis, C. A. Schmidt, S. N. Patek, X. Zhang, N. D. Tsutsui, A. V. Suarez, Phylogeny, scaling, and the generation of extreme forces in trap-jaw ants. *J. Exp. Biol.* **211**, 2358–2368 (2008). doi:10.1242/jeb.015263 Medline

147. M. A. Seid, R. H. Scheffrahn, J. E. Niven, The rapid mandible strike of a termite soldier. *Curr. Biol.* **18**, R1049–R1050 (2008). doi:10.1016/j.cub.2008.09.033 Medline

148. M. Burrows, M. Dorosenko, Jumping mechanisms and strategies in moths (Lepidoptera). *J. Exp. Biol.* **218**, 1655–1666 (2015). doi:10.1242/jeb.120741 Medline

149. M. J. Medeiros, R. Dudley, Jumping performance in flightless Hawaiian grasshopper moths (Xyloryctidae: *Thyrocopa* spp.). *Proc. Hawaii. Entomol. Soc.* **44**, 55–61 (2012).

150. M. Burrows, Jumping mechanisms and performance of snow fleas (Mecoptera, Boreidae). *J. Exp. Biol.* **214**, 2362–2374 (2011). doi:10.1242/jeb.056689 Medline

151. M. Burrows, M. Dorosenko, Jumping mechanisms in lacewings (Neuroptera, Chrysopidae and Hemerobiidae). *J. Exp. Biol.* **217**, 4252–4261 (2014). doi:10.1242/jeb.110841 Medline

152. Y. Tanaka, M. Hisada, The hydraulic mechanism of the predatory strike in dragonfly larvae. *J. Exp. Biol.* **88**, 1–19 (1980).

153. M. Burrows, H. Wolf, Jumping and kicking in the false stick insect Prosarthria teretrirostris: Kinematics and motor control. *J. Exp. Biol.* **205**, 1519–1530 (2002). Medline

154. M. Burrows, O. Morris, Jumping and kicking in bush crickets. *J. Exp. Biol.* **206**, 1035–1049 (2003). doi:10.1242/jeb.00214 Medline

155. M. Burrows, O. Morris, Jumping in a winged stick insect. *J. Exp. Biol.* **205**, 2399–2412 (2002). Medline

156. H. C. Bennet-Clark, E. C. A. Lucey, The jump of the flea: A study of the energetics and a model of the mechanism. *J. Exp. Biol.* **47**, 59–67 (1967). Medline

157. M. Burrows, M. Dorosenko, Jumping mechanisms in adult caddis flies (Insecta, Trichoptera). *J. Exp. Biol.* **218**, 2764–2774 (2015). doi:10.1242/jeb.123471 Medline

158. L. Yafetto, L. Carroll, Y. Cui, D. J. Davis, M. W. F. Fischer, A. C. Henterly, J. D. Kessler, H. A. Kilroy, J. B. Shidler, J. L. Stolze-Rybczynski, Z. Sugawara, N. P. Money, The fastest flights in nature: High-speed spore discharge mechanisms among fungi. *PLOS ONE* **3**, e3237 (2008). doi:10.1371/journal.pone.0003237 Medline

159. M. Fischer, J. Cox, D. J. Davis, A. Wagner, R. Taylor, A. J. Huerta, N. P. Money, New information on the mechanism of forcible ascospore discharge from Ascobolus immersus. *Fungal Genet. Biol.* **41**, 698–707 (2004). doi:10.1016/j.fgb.2004.03.005 Medline

160. J. L. Stolze-Rybczynski, Y. Cui, M. H. H. Stevens, D. J. Davis, M. W. F. Fischer, N. P. Money, Adaptation of the spore discharge mechanism in the basidiomycota. *PLOS ONE* **4**, e4163 (2009). doi:10.1371/journal.pone.0004163 Medline

161. J. C. R. Turner, J. Webster, Mass and momentum transfer on the small scale: How do mushrooms shed their spores? *Chem. Eng. Sci.* **46**, 1145–1149 (1991). doi:10.1016/0009-2509(91)85107-9

162. R. S. Wilson, C. E. Franklin, R. S. James, Allometric scaling relationships of jumping performance in the striped marsh frog *Limnodynastes peronii*. *J. Exp. Biol.* **203**, 1937–1946 (2000). Medline

163. V. A. Tucker, T. J. Cade, A. E. Tucker, Diving speeds and angles of a gyrfalcon (*Falco rusticolus*). *J. Exp. Biol.* **201**, 2061–2070 (1998). Medline

164. A. M. Wilson, J. C. Lowe, K. Roskilly, P. E. Hudson, K. A. Golabek, J. W. McNutt, Locomotion dynamics of hunting in wild cheetahs. *Nature* **498**, 185–189 (2013). doi:10.1038/nature12295 Medline

165. J. F. Campbell, H. K. Kaya, Mechanism, kinematic performance, and fitness consequences of jumping behavior in entomopathogenic nematodes (*Steinernema* spp.). *Can. J. Zool.* **77**, 1947–1955 (1999). doi:10.1139/z99-178